Photochemical internalization (PCI) of sunitinib: efficacy and impact on sunitinib resistance

Judith Jing Wen Wong

Master's thesis
Department of pharmacy
School of Pharmacy
Faculty of Mathematics and Natural Sciences

UNIVERSITY OF OSLO

May 2016

Photochemical internalization (PCI) of sunitinib: efficacy and impact on sunitinib resistance

Judith Jing Wen Wong

Supervisors

Dr. Anette Weyergang,

dr. Maria Elisabeth Brandal Berstad

and professor Kristian Berg

Department of Radiation Biology

Institute for Cancer Research – The Norwegian Radium Hospital

Oslo University Hospital

UiO : School of Pharmacy
University of Oslo

Oslo University Hospital

2016

Photochemical internalization (PCI) of sunitinib: efficacy and impact on sunitinib resistance

Judith Jing Wen Wong

http://www.duo.uio.no/

Print: Reprosentralen, University of Oslo

Abstract

The cancer cells ability to develop resistance toward therapy is a major clinical problem, and is one of the main reasons why cancer remains difficult to cure [1]. Tyrosine kinase inhibitors (TKIs) is a group of novel cancer therapeutics that specifically interfers with cellular signalling pathways that are involved in critical processes [2, 3]. These signalling pathways are important for tumor cell proliferation and survival [2, 3]. TKIs have emerged as one of the most intensively pursued targets in cancer therapeutics. The first TKI was approved in 2001 and by the end of 2015, 30 TKIs had gained FDA approval [4]. Although these therapeutics are more specific compared to traditional chemotherapeutics, development of drug resistance has emerged as a considerable problem in patients receiving TKIs [5]. Photochemical internalization (PCI) is a novel technology for release of therapeutics sequestered in vesicles into the cytosol [1]. It is based on the use of photosentiziser (PS) localized in the membrane of endocytic vesicles, ruptures the membrane upon light exposure, and thereby release of entrapped therapeutics [1]. PCI has been indicated as a strategy to overcome resistance, and has been documented both *in vitro* and *in vivo* [1] .

In this current thesis, HT-29 cells, human colorectal adenocarcinoma, was used as a research model. A sunitinib-resistant HT-29 cell line was established by continous exposure of sunitinib, a TKI, for 1-5 months. $TPCS_{2a}$, which is a clinical relevant PS, was used in this thesis. Sunitinib was found to be localized in lysosomes in both parental and sunitinib-resistant HT-29 cells, and PCI was explored as a potential strategy for cytosolic sunitinib release. Treatment with PCI with “light after”-procedure did not potentiate the toxic effect of sunitinib in neither of the cell lines. This is the procedure where the cells are incubated with sunitinib and $TPCS_{2a}$ before illumination. It was proposed that the reactive oxygen species (ROS) generated during the photochemical reaction destroyed sunitinib. The PCI-procedure was therefore changed to “light first”, where the cells were subjected to sunitinib immediately after illuination. A PCI effect could be observed with the “light first”-procedure in parental HT-29 cells. The same effect could, however, not be observed in sunitinib-resistant HT-29 cells. The cells were also subjected to PCI of rGel, a recombinant plant toxin, where similar effect could be observed in both cell lines. The present study rejects PCI as an approach to overcome sunitinib resistance. However, the sunitinib-resistant cells were not found to be cross-resistant to PCI in general, and PCI of rGel is here indicated as a strategy to circumvent sunitinib resistance.

Acknowledgements

The work presented in this thesis was carried out at the Department of Radiation Biology, Institute for Cancer Research at the Norwegian Radium Hospital, Oslo University Hospital in the time period of August 2015 to May 2016. This a thesis for the Master's degree in Pharmacy at the School of Pharmacy, University of Oslo. It has been a period of intensive learning, both in the scientific arena and on a personal level. Several people have supported and helped me throughout this period.

First of all, I would like to express my great appreciation to my supervisors Anette Weyergang, Maria Elisabeth Brandal Berstad and Kristian Berg. This thesis has been carried out under the supervision of my main supervisor, Anette Weyergang, who I would like to thank for excellent guidance and encouraging words. I would also like to thank Maria Elisabeth Brandal Berstad for being patient, always taking the time to help and planning the experiments. And last, but not least, I wish to acknowledge the help and valuable input provided by Kristian Berg.

A special thanks should be given to Ane Sofie Viset Fremstedal for her skilled assistance and supervision of work in the laboratory. My sincere thanks also goes to Pål Selbo for sharing his expertise in fluorescence microscopy, and Cathrine Elisabeth Olsen for generously helping me with flow cytometry. I am also thankful to the rest of the PCI group for creating a friendly working environment.

Finally, I wish to thank my boyfriend Vu Nguyen and my family for their continuous support and encouragements that have helped me to stay focused and motivated. I am also grateful to my friends and fellow students who have made this period a lot more fun.

Oslo, May 2016

Table of Contents

Abbreviations

ABC	ATP-binding casette
AMD	Age-related macular degeneration
ALA	5-aminolevunic acid
$AlPcS_{2a}$	Aluminium phatlocyanine disulfonate
ATP	Adenosine triphosphate
BCRP	Breast cancer resistance protein
DC	Dendritic cell
DMSO	Dimethyl sulfoxide
EC	Endothelial cell
EGFR	Epithelial growth factor receptor
FDA	US Food and Drug Administration
FSC	Forward-scattered light
GIST	Gastrointestinal stromal tumor
HIF-1	Hypoxia Inducible Factor
Hp	Hemaetoporphyrin
HpD	Hemaetoporphyrin derivate
HT-29/SR	Sunitinib-resistant HT-29
HT-29/PAR	Parental HT-29
ISC	Intersystem crossing
LAMP	Lysosome-associated membrane glycoprotein
MDR	Multidrug resistance
MRP1	Multidrug resistance-associated protein
MTT	3-(4,5-dimethylthiazol-2-yl)-2,5-diphenyltetrazolium bromide

PBS	Phosphate buffered saline
PCI	Photochemical internalization
PDGF	Platelet-derived growth factor
PDGFR	Platelet-derived growth factor receptor
PDT	Photodynamic therapy
Pgp	P-glycoprotein
PpIX	Protoporhyrin IX
PS	Photosensitizer
pVHL	Von Hippel-Lindau protein
RIP	Ribosome-inactivating protein
rGel	Recombinant gelonin
ROS	Reactive oxygen species
RTK	Receptor tyrosine kinase
SSC	Side-scattered light
TFEB	Transcription factor EB
TKI	Tyrosine kinase inhibitor
$TPCS_{2a}$	Meso-tetraphenyl chlorin disulphonate
$TPPCS_{2a}$	Meso-tetraphenyl porphyrin disulphonate
VEGF	Vascular endothelial growth factor
VEGFR	Vascular endothelial growth factor receptor

Aim of the study

Research in the field of oncology has across the last decades revolutionized our understanding of cancer. The increasing understanding of cancer has lead to development of new therapeutics that are more specific compared to traditional chemotherapeutic agents. Despite the fact that new cancer therapeutics are more specific, drug resistance is a still a major challenge and a source of therapeutic failure [6]. Antiangiogenic tyrosine kinase inhibitors (TKIs) are a novel group of cancer therapeutics. These TKIs are small enough to penetrate the cell membrane and act on intracellular targets in cancer cells involved in growth, proliferation and survival of cancer cell in addition to their action on endothelial cells (ECs) [3].

Sunitinib is an anti-angiogenic TKI that is approved in Norway (Sutent®, Pfizer) for gastrointestinal stromal tumor (GIST), metastatic renal cell carcinoma and pancreatic neuroendocrine tumors [7]. Intially, resistance to TKIs was not expected as these are designed to target ECs and other stromal cells, which are genomically stable and therefore unlikely to develop mutations [3, 8] Unfortunately this was not the case as most patients developed resistance during treatment. There are many mechanisms that can be involved in sunitinib resistance. Recently, Gotink *et al.* identified lysosomal sequestration as a resistance mechanism for sunitinib [9].

The aim of this study was to investigate if photochemical internalization (PCI) could be used as a stratetgy to circumvent resistance in sunitinib-resistant HT-29 cells. Photochemical internalization (PCI) is a drug delivery system for cytosolic release of drugs that are trapped in endocytic vesicles [1]. HT-29 cancer cells with origin from human colorectal adenocarcinoma were used as research model [10].

1 Introduction

1.1 Drug resistance in cancer

Over the last decades, significant progresses have been made in the field of oncology leading to longer patient survival and improved quality of life. Despite major advances in cancer treatment, drug resistance remains one of the leading causes of treatment failure [6]. Multidrug resistance (MDR) is a phenomenon that occurs when cancer cells develop resistance to classes of cancer therapeutics that are structurally and mechanistically unrelated [11]. MDR can be divided into two broad categories: intrinsic and aqcuired. Intrinsic resistance are resistance-mediating factors that pre-exist in a population of tumor cells before treatment leading to ineffective therapy. Acquired resistance is caused by mutation arising during treatment [12, 13]. MDR is further complicated by the genetically heterogeneous composition of a tumor. This can give rise to different MDR mechamisms in different populations of cancer cells within the same tumor. This phenomenon is known as multifactorial MDR [12].

The mechanisms contributing to MDR have been studied extensively and are complex; increased drug efflux, alteration and mutation of drug target, and lysosomal sequestration are some of the identified mechanisms in cancer cells [13]. Enhanced drug efflux may be linked to increased expression of cell membrane transporter proteins, most notably the ATP-binding casette (ABC) transporter family [13]. These transmembrane proteins regulate the flux of molecules across the plasma membrane [13]. Although many of transporters have been linked to MDR, they are all also expressed in normal tissues where they have an important role in the regulation of central nervous system permeability, and also protecting the brain against blood-born potentially harmful chemicals by the blood-brain barrier and the blood-cerebrospinal-fluid barrier [13]. ABC transporter proteins can also be found on the surface of epithelial cells that have excretory roles, including small intenstines, lining of colon and kidney proximal tubules [13, 14].

Three proteins from the ABC transporter family have been studied extensively in relation to MDR; P-glycoprotein (P-gp), MDR-associated protein (MRP1) and breast cancer resistance protein (BCRP) [11, 13]. P-gp is overexpressed in many tumors and can also be induced by cancer therapeutics [13]. Overexpression of P-gp has been associated with therapeutic failure

in different types of cancer, including colon, liver and kidney cancers, as well as leukemias and lymphomas [12, 13]. Recently it has been shown that targeted TKIs such as sunitinib, imatinib, erlotinib and nilotinib are also substrates and modulators of P-gp and BCRP [15].

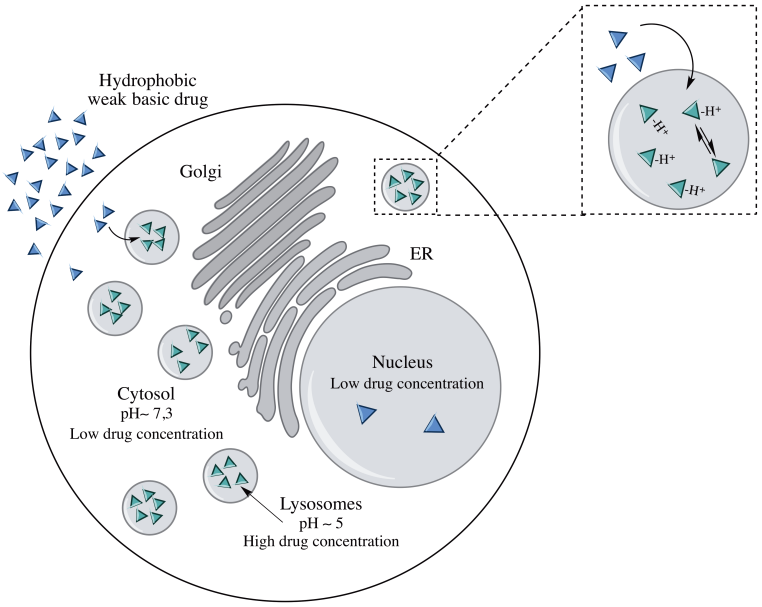

Figure 1 | **Lysosomal sequestration of hydrophobic weak basic drug.** The drug molecules diffuse freely across the plasma and lysosomal membrane. In lysosomes the molecules become protonated (represented in the figure by H^+) and therefore unable to cross the lipid lysosomal membrane, leading to lysosomal accumulation. The drug concentration is reduced in the cytosol and nucleus. Adapted from Zhitomirsky and Assaraf (2016) [16].

Another mechanism related to MDR is lysosomal sequestration, a process where hydrophobic, weak basic drugs are accumulated in acidic lysosomes (fig.1) [16]. Lysosomes are central, acidic organelles that partake in a number of physiological processeses including degradation of endocytosed macromolecules and worn out organelles [17]. At physiological pH, weak basic hydrophobic drugs are able to travel freely across lipid membranes, including both plasma and lysosomal membranes. However, when these drugs are subjected to the acidic pH in lysosomes (pH~5) protonation occurs and the drugs become unable to traverse the lipid lysosomal membrane. Lysosomal sequestered drugs are unable to reach their cytosolic targets, this leading to lower drug concentration at target site. It has previously been described that exposure of lysosomal-accumulating cancer therapeutics can induce lysosomal biogenesis in cancer cells [16]. Lysosomal biogenesis is the process where lysosomes are generated as part of the degradative endocytic pathway [18]. Endocytosed cargo passes through a range of endosomal intermediates, where lysosomes is the terminal station for the degradative endocytic pathway [17, 18]. This has been found to be mediated through the transcription factor EB (TFEB), the master regulator of lysosomal biogenesis [18]. TFEB activation leads to increased lysosomal

biogenesis and elevated number of lysosomes [16]. In 786-O renal cancer cells and HT-29 colorectal cancer cells, it has previously been reported that continuous exposure to sunitinib leads to increased lysosomal capacity [9]. Several other cancer therapeutics have also been shown to undergo lysosomal sequestration including doxorubicin, daunorubicine, vincristine, mitoxantrone, gefitinib and lapatinib [16].

While lysosomal sequestration of cancer therapeutics prevents the drugs to reach their intracellular target, clearance of lysosome-sequestrered drugs by exocytosis provides an additional line of defense. Lysosomal exocytosis is the process where the lysosomes fuse with the plasma membrane to release their cargo into the extracellular space, this has been suggested as a mechanism in clearance of lysosome-sequestered drugs [16].

Passive accumulation remains the primary mechanism suggested for lysosomal drug sequestration, but it has been reported that ABC transporters may be involved in active lysosomal drug sequestration [16]. P-gp is not only localized in the plasma membrane, but also in vesicle membrane [16, 19].

1.2 Tumor angiogenesis

Cancer cells grow and proliferate uncontrollably and are able to invade the surrounding tissue and colonize in distant organs [20]. A number of essential hallmarks of cancer that drive tumorgenesis have been identified and includes resisting cell death, sustaining proliferative signaling, enabling replicative immorality, activating invasion and metastasis, evading growth suppressors and inducing angiogenesis [21].

Angiogenesis is the sprouting of a new vessel from pre-existing vasculature [8]. Normally, angiogenesis is well controlled by pro- and antiangiogenic factors, and is a transient physiological process [8]. At normal physiological condition, angiogenesis is only promoted during wound healing and repair, pregnancy and female reproductive cycle [8]. However, in cancer, an adequate blood supply is required for sufficient oxygen and nutrients to support rapid tumor growth [8]. Tumor angiogenesis is induced by secretion of pro-angiogenic signals from the tumor itselves. These signals are produced in response to hypoxia, usually when the tumor reaches the critical size of 1-2 mm in diameter, recognized as the “angiogenic switch” [20]. These pro-angiogenic signals are endogenous ligands for receptors present on the endothelial cell’s (EC’s) surface [22]. Upon ligand binding, intracellular transductions and gene

transcriptions are initiated resulting in EC proliferation and invasion [22]. Activated ECs secrete protease to degrade the basement membrane to detach their junctional adhesion, migrate, and interact with surrounding stroma [5, 22]. New blood vessels are formed toward gradients of proangiogenic factors where ECs form tube-like structures and stromal cells are recruited to support the structure [5, 22]. During tumor progression, an "angiogenic switch" is almost always activated and sustained to support tumor growth [21]. The sustained and elevated angiogenic mediators does not allow the production of mature and proper blood vessels to improve hypoxia [22]. The resulting vasculature is both structurally and functionally abnormal. Tumor blood vessels are dilated, saccular, tortous and leaky [21, 22]. These vessels does not only function to supply the tumor with nutrients and oxygen, but also provide an escape route for tumor cells to form micromestasis [20].

Major mediators of tumor angiogenesis

There are many molecules that have been implicated as positive regulators of tumor angiogenesis. Although several pro-angiogenic factors are identified, there is a consensus that vascular endothelial growth factor (VEGF) is one of the major mediators of this process [23]. The VEGF family is comprised of VEGF-A, -B, -C, -D, -E and placenta growth factor [5]. VEGF-A is the key regulator of blood vessels and growth, whereas VEGF-C and VEGF-D regulate lymphatic angiogenesis [23].

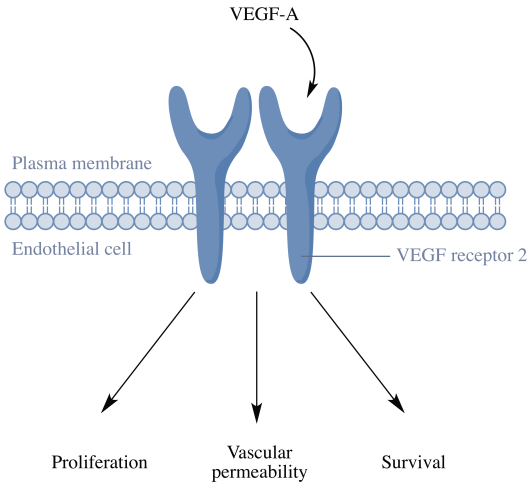

Figure 2 | **A simplified overview of the biological effects of vascular endothelial growth factor A (VEGF-A).** Adapted from Kerbel (2008) [24]

VEGF-A, hereinafter referred to as VEGF, signals mainly through VEGF receptor 2 which is expressed at elevated levels by ECs that are engaged in tumor angiogenesis (fig. 2) [24]. Other

effects of VEGF include vascular permeability and prosurvival effects (fig. 2) [5]. In many human cancer cells, the level of VEGF is elevated [24]. Upregulated VEGF expression has been observed in human colorectal adenocarcinoma and has been linked to poor prognosis and metastatic spreading [5]. This is likely induced both by epigenetic and genetic changes. Epigenetic factors such as hypoxia, low pH and inflammatory cytokines (e.g. interleukin 6) can induce or increase VEGF expression [24]. Genetic changes are activation of oncogenes or loss/mutational inactivation of tumor-suppressor genes, for instance the tumor-suppressor gene Von Hippel-Lindau (VHL) [24].

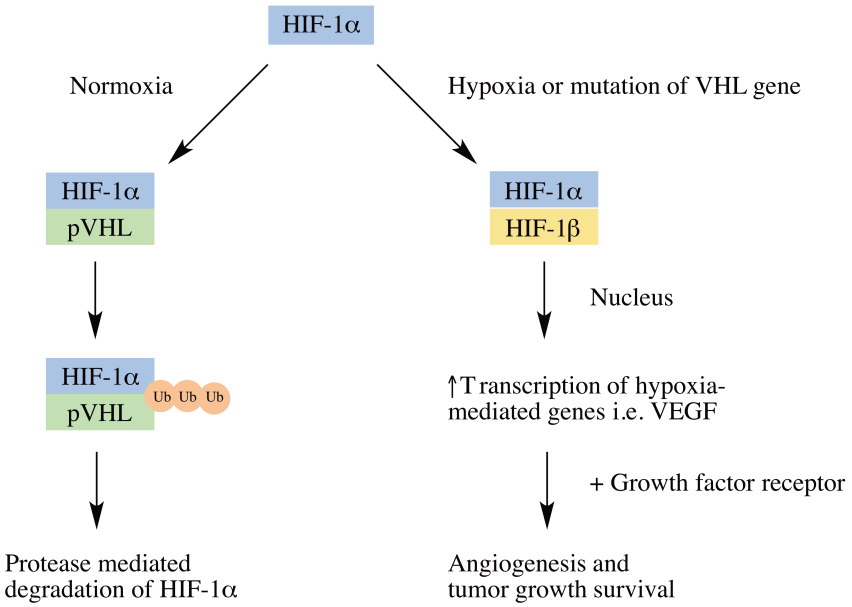

Figure 3 | **Oxygen-dependent HIF-1α regulation**. In normoxic conditions, HIF-1α is recognized by Von Hippel-Lindau protein (pVHL) and targeted for ubiquitylation (Ub) and protease mediated degradation. Under hypoxic conditions or inactivation of VHL gene, HIF-1α forms heterodimer with HIF-1β and translocate to the nucleus to induce transcription of genes involved in angiogenesis. Adapted from Gossage *et al*. (2015) [25]

Proteins encoded from the VHL gene have a critial role in regulation of the key transcription factor involved in angiogenesis, hypoxia inducible factor-1 (HIF-1) (fig. 3) [26]. This transcription factor is responsible for the transcribing genes that encode pro-angiogenic factors, including VEGF [23]. HIF-1 is a heterodimer transcription factor consisting of an α- and β-subunit. The HIF-1 β-subunit is constitutively expressed, whereas the HIF-1 α-subunit is increases in response to hypoxia [27]. HIF-1α is under normoxic conditions targeted for ubiquitination and rapid degradation in cytosol. However, under hypoxic conditions the α- and β-subunit of HIF-1 will dimerize and can enter the nucleus to activate transcription [26, 27]. The VHL tumor suppressor protein (pVHL) provides a negative regulation of VEGF and other pro-angiogenic mediators [23]. The importance of pVHL is indicated in the rare inherited *VHL*

syndrom where the gene is mutated. This is a neoplastic disease that is associated with various tumor types, including clear-cell renal cell carcinoma, central nervous system and retinal haemangioblastomas, and pancreatic neuroendocrine tumors [23, 25].

A second important mediator of angiogenesis is the platelet derived growth factor (PDGF). The PDGF family comprise of four members: PDGF-A-, B-, C- and -D [3]. PDGF-A, hereinafter referred to as PDGF, is a powerful chemoattractant on ECs and necessary for the maturation and stability of the vasculature [5]. It also facilitates recruitment of pericytes and smooth muscle cells [28]. It has been hypothesized that human colorectal tumors with low levels of VEGF expression are more dependent of PDGF as the major proangiogenic mediator [5]. Similar to VEGF, the expression of PDGF by tumors have been linked to poor prognosis in gastric and pancreatic cancer [5].

1.3 Tyrosine Kinase Inhibitors (TKIs)

1.3.1 Receptor tyrosine kinases (RTKs)

Protein phosphorylation is an important mechanism in signal tranduction pathways [2]. This phosphorylation is carried out by protein kinases which are involved in the regulation of fundamental cellular processes including proliferation, differentiation, migration and survival [2, 29]. Protein kinases can be classified into tyrosine kinases, serine/threonine kinases and atypical kinases (fig. 4) [3]. This classification is based on which residue of the protein kinase that is phosphorylated. There are approximately 30 families of tyrosine kinases [3]. Protein kinases can also be classified on basis of their cellular localization: receptor kinases and non-receptor kinases [3]. RTKs are a main focus in the present thesis. RTKs are essential for extracellular signal transduction into the cell, whereas non-receptor tyrosine kinases are responsible for the intracellular signalling [3]. RTKs are transmembrane proteins with an extracellular domain for ligand –binding and an intracellular domain that possess tyrosine kinase activity [2, 30]. The kinase domain comprises two lobes that forms an ATP-binding cleft [2, 3]. Upon ligand binding, RTKs dimerize or multimerize which leads to conformational changes that gives ATP access to the ATP-binding cleft [30]. Binding of ATP results in autophosphorylation of specific tyrosine residues at the kinase domain [2, 30]. Adaptor proteins are recruited to the activated RTK where they bind to phosphorylation sites and initiates a complex system of signaling cascades [3, 30].

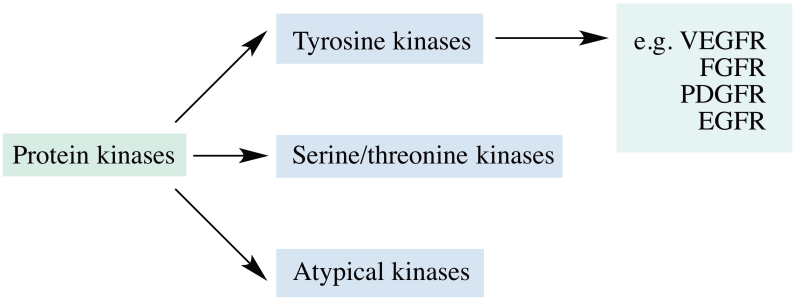

Figure 4 | **Classification of protein kinases.** Protein kinases can be divided into tyrosine and serine/threonine kinases. There are approximately 30 families of tyrosine kinases. VEGFR: vacular endothelial growth factor, FGFR: fibroblast growth factor, PDGFR: platelet-derived growth factor receptor, EGFR: epidermal growth factor receptor. Adapted from Gotink and Verheul (2011) [3].

A number of intracellular signaling cascades can be activated, including the mitogen-activated protein kinase (MAPK), phosphoinositol-3 kinase (P13K)/Akt and protein kinase C (PKC) pathways which leads to transciptional responses [2, 3]. A general response in the activation of cell-surface-receptors, inluding RTKs, is internalization [2]. This involves endocytosis of occupied receptors. Depending on the receptor and ligand pair, RTKs can be recycled from endosomes back to the plasma membrane or follow the endocytic pathway to lysosomes for degradation [31].

1.3.2 TKIs: Mechanism of action

RTKs are involved in cellular signalling pathways that regulate several critical processes that are important for tumor progression[30]. Dysregulated signalling of RTKs has been implicated in cancer progression and tumor metastasis [30]. TKIs are small molecules and are able to pass the cell membrane due to both their size and hydrophilicity [3]. In the cell they can interact with the intracellular domain of tyrosine kinase receptors and block the activation of various downstream signaling pathways [3, 32]. The dysregulated RTK signalling can be mediated by a number of mechanisms, where the most common mechanisms are chromosome rearrangement, RTK overexpression and gain-of-function mutations [33]. The first FDA approved TKI was imatinib (Gleevec®, Novartis) in 2001, a Bcr-Abl inhibitor [34]. The Bcr-Abl fusion protein is caused by a chromosomal translocation between chomosome 9 and 22, known as the *Philadelphia chromosome*, which is tightly associated with chronic myelogenous leukemia [35].

However, it is not only RTK expression by tumor cells that kan drive tumor progression, additional cell types also play a significant role. In particular, VEGF receptor-2 and PDGF

receptor-β located on EC and pericytes, respectively, play a crucial role in tumor angiogenesis [30]. Anti-angiogenic TKIs have therefore been developed as a systemic treatment strategy for cancer [3]. By the end of 2015, a total 30 of small-molecule kinase inhibitors had gained FDA approval, where seven of these are anti-angiogenic with VEGFR as their primary target [4, 34]. Most of the anti-angiogenic TKIs are ATP mimetics and compete with ATP for binding at the kinase domain of the receptor [3, 36]. They are also so-called multi-targeted kinase inhibitors and designed to target EGFR, PDGFR and VEGFR [3, 29]. As a result they are able to target a various number of kinases and inhibit several signalling pathways. For inhibition of angiogenesis, a multi-targeted TKI blocking both EGFR and PDGFR is thought to be more effective than targeting only one of these pathways [3]. As a result of the broad target range, there is also a risk of "off-targets" leading to side-effects and toxicity [3, 37].

Sunitinib

Sunitinib malate (Sutent®, Pfizer) (fig. 5) is an oral, multi-targeted TKI that have affinity for VEGFR-1, -2, -3, PDGFR, stem cell factor receptor (KIT), glia cell-line derived neurotrophic factor receptor (RET), FMS-like tyrosine kinase-3 (FLT3) and the receptor for macrophage colony-stimulating factor (CSF-1R) [30, 38]. Originally, expression of VEGFRs was thought to be limited to ECs, however it is now known that VEGFRs are expressed by a number of tumor types [39]. Anti-angiogenic TKIs can also target VEGFRs on tumor cells. Sunitinib inhibits both proliferation and clonogenic capacity directly in tumor cells [3, 30]. Pre-clinical data indicated that the direct antiproliferative actitivity of sunitinib is dependent upon prescence of constitutively active RTKs in tumor cells [30].

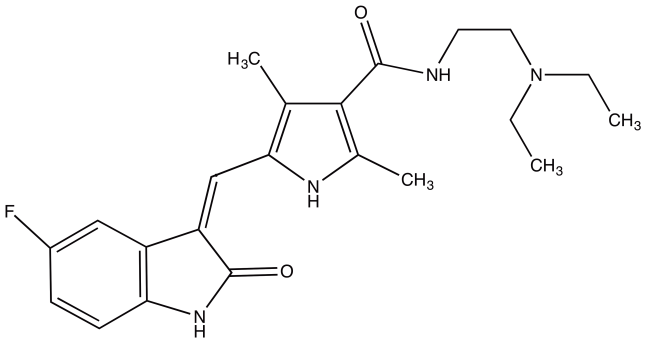

Figure 5 | **Chemical structure of sunitinib.** Sunitinib is a weak base with a pK_a value of 9,04 and log P = 2,93-3,24 [40].

Although anti-angiogenic TKIs can induce dramatic clinical responses in treated patients, the benefit is limited by development of drug resistance leading to disease progression [3, 41]. Mechanisms of acquired resistance could be induced by alternative signaling of tumor cells including production of alternative angiogenic growth factors [3]. Since sunitinib can also target tumor cells, mutations at target receptors is also a possible resistance mechanism. Several studies have reported mutations in target kinases that correlate with resistance to sunitinib in GIST [3]. Sunitinib restistance of tumor cells can also be mediated by increased lysosomal sequestration [9, 16]. Sunitinib is a weak base and lipophilic with a pK_a value of 9,04 and log P = 2,93-3,24 [40]. There is also a small fraction of patients that do not respond to the anti-angiogenic treatment due to intrinsic resistance [3].

1.4 PDT – Photodynamic Therapy

Photodynamic therapy (PDT) is a treatment modality for both oncogenic and non-malignant diseases which requires three components: light, a photosensitizer (PS) and oxygen [42]. None of these components are toxic by themselves, but when combined they can produce reactive oxygen species (ROS) [43]. Production of ROS can cause cellular toxicity and induce apoptosis, necrosis or autophagy in cells [44]. PDT can also cause tumor vasculature destruction and induce an inflammatory response that further lead to activation of an immune response [42, 44].

The first *in vitro* photodynamic effect was observed by the medical student Oscar Raab with his Professor Herman Von Tappeiner in Germany, at the dawn of the 20th century. This observation led to investigation of the dermatological applications where the first attempts to use PDT to treat tumors and skin conditions were performed with favorable results [45]. The importance of light, PS and oxygen was documented and the term “photodynamic effect” was used to describe this phenomen. However, PDT was not clinically tested until a half of a century later. In the 1950s, in the United States, Dr. Sam Schwartz observed that crude preparations of hemaetoporphyrin (Hp) tended to localize at sites of neoplasia. Fluorescence of the accumulated Hp could be detected by UV-light [46].

However, it was also discovered that Hp typically used was not exclusively a Hp solution, but an impure mixture. Lipson and colleagues tried to purify Hp, and instead of isolating a purifed compound they made a mixture of monomers and oligomers – hemaetoporphyrin derivate (HpD) [44, 45, 47]. Sodium porfimer, the first PS that later achieved clinical apporval, is a

refined HpD where the number of monomers are reduced [46]. With the help of Dr. Thomas Doughtery, both preclinical and clinical studies quickly expanded in the 70s to investigate the potential of HpD. These studies eventually led to drug approval. HpD was first given approval in 1993 by the Candadian health agency and later in other countries [48, 49].

1.4.1 Photosensitizers (PS)

The PS is an important component in PDT. This is a chemical or synthethic compound that has the ability to absorb a photon of visible light and transfer the absorbed energy to another molecule. The absorbed energy is in general thought to be transferred to molecular oxygen nearby, and subsequently inducing production of ROS [47]. PS can in general accumulate in cellular and subcellular membranes both in tissue and vasculature. The intracellular localization of the PS is dependent on its chemical properties. Hydrophobic PS diffuse across the plasma membrane and accumulate in various subcellular compartments such as lysosomes, plasmic membrane, mitochondria, endoplasmic reticulum, Golgi apparatus, or combination of these [50]. Amphiphilic PSs, as used in the present thesis, are taken up by the cells by means of endocytosis and accumulates in the endo/lysosomal membranes [1]. The PSs used in oncology are negatively charged and are not found to be localized in nucleus, it is therefore considered as a non-mutagenic cancer treatment as it does not affect DNA [42, 50].

The subcellular damage of PDT is linked to the site where the PS is located. The half life of singlet oxygen in biological systems is estimated to be approximately 40 nanoseconds and in cellular environment singlet oxygen can only diffuse about 10-20 nm [51]. The singlet oxygen can therefore in theory only interact with molecules and structures within its diffusion radius [49]. One of the advantages of PDT in oncolgy is the preferential accumulation of PS in tumor and tumorvasculature [42, 52]. This allow differential concentration of the PS between normal tissue and tumor, thus leading to a restricted photo-induced damage in the surrounding normal tissue [42]. The preferential accumulation of PS may be explained by the increased vascular permeability in tumors in addition to a reduced lymphatic drainage which together favors retention of the PS [52, 53]. In addition, the extracellular compartment of the tumor has a decreased pH [52]. The PS may therefore be subjected to protonation, making it more lipophilip as it enters the tumor. There is also an elevated level of low-density lipoprotein receptor expression on tumor surface which favors PS accumulation [53].

There are several characteristics an ideal PS should have in order to be useful in clinical settings. An ideal PS should have low dark toxicity, rapid elimination from normal tissue to avoid prolonged photosensitization and absorption of light at longer wavelength (~ 600-900 nm) for sufficient tissue penetration [54].

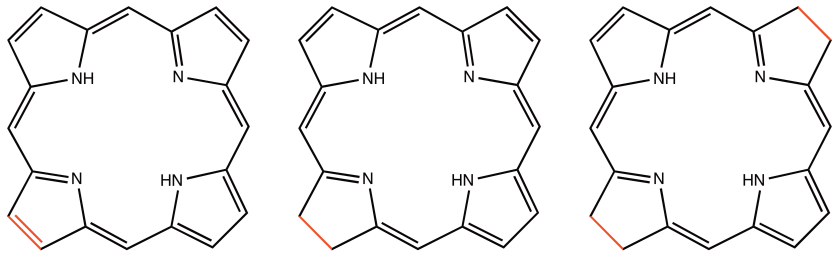

Porphyrin Chlorin Bacteriochlorin

Figure 6 | **Chemical structures of porphyrin, chlorin and bacteriochlorin**. Many PS have a structure based on porphyrin or chlorin. Porphyrins with one reduced double bond is named chlorin, and two reduced double bonds are bacteriochlorin. Adapted from Berg (2009) [47]

A variety of compounds may behave as a PS and a great number of potential PS have been developed towards clinical applications. However, only a few PSs have made it to clinical trials and even fewer are currently approved [54]. Photofrin® (porfimer sodium) is a porphyrin-based PS with the longest clinical history and patient track record. Some of the drawbacks associated with Photofrin® are batch-to-batch variations due to its complex composition, prolonged photosensitization, and low absorption maximum (632 nm) which limits the effective tissue penetration [55].

Most of the PS used in PDT have a structure based on porphyrin or porphyrin-related compounds (fig. 6). Porphyrin is composed of four pyrrole subunits that are connected by methine bridges [47]. Porphyrins with one reduced double bond are named chlorins, and two reduced double bonds are bacteriochlorin (fig. 6) [47]. Reduction of one or two double bonds in the conjugated ring structure or extending the number of conjugated double bonds in the ring system can increase the absorption maximum in the red wavelength region [47, 49]. *In vivo* studies have indicated that the shift in the red wavlenth region increases in the following sequence; porphyrin, chlorin and bacteroichlorin [56].

Examples of clinically available porphyrin-based PSs are Visudyne® (verteporfin), Levulan® (5-aminolevunic acid, ALA) and Metvix® (ALA-methyl ester). Visudyne® is approved for age-related macular degeneration (AMD), however not clinically approved in oncology. A

phase I/II study with PDT using verteporfin has been carried out in pancreatic cancer patients where Huggett *et al.* concluded that median survival was comparable to patients treated conventially [57, 58]. ALA and ALA-methyl ester are prodrugs that take advantage of the body's biosynthetic capability to produce protoporphyrin IX (PpIX) which is a PS. The rate-limiting step in the heme biosynthesis is the convertion of glycine and succinyl coenzyme-A to ALA [56]. Enhancing the ALA concentration leads to accumulation of porphyrins, mainly PpIX, the immediate precursor of heme. Heme itself is not a PS due to the coordinated Fe^{2+} in the centre [47, 56]. Both Levulan® and Metvix® are approved for treatment of actinic keratosis. Metvix® is also approved for basal cell carcinoma and Bowen's disease. Levulan® and Metvix® are formulated as cream and administered topically [47, 59]. Hexvix® (ALA-hexyl ester), a systemic drug, takes advantage of PpIX-based fluorescence and is approved for detection of bladder cancer *in situ* [47].

Foscan® (temoporfin) is a chlorin-based PS clinically used with PDT [54]. It is approved for treatment of squamous cell carcinomas of head and neck [47]. Temoporfin has several attractive properties including synthetic purity and high quantum yield, meaning it effectively transform molecular oxygen to singlet oxygen [42]. Temoporfin is considered one of the most effective clinically used PSs with treatment time measured in seconds to minutes [42, 60].

1.4.2 Photochemical reactions

A PS exists in a ground state and is activated when exposed to light at a specific wavelength corresponding to its absorption peak [45]. Once the excitation occurs, the PS is in a singlet state which is an unstable and transient state [45]. Several processes may occur when the PS is in singlet state, the excited PS can return to ground state and loose the energy by fluorescence or heat [61]. Another process that can take place and is characteristic for PDT is intersystem crossing (ISC) (fig. 7) [61].

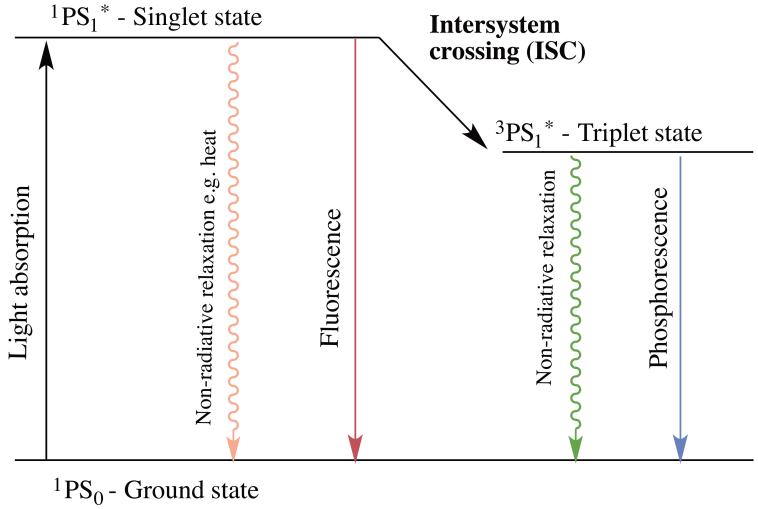

Figure 7 | **Simplified Jablonski diagram.** This diagram shows the photoactivation and photophysical deactivation processes that can occur following light absorption. Adapted from Craig *et al.* (2015) [62]

The PS, by ISC is converted to a triplet state. This state is favored as it is of lower energy compared to the singlet state [45, 56]. Triplet state is a relatively long-lived state (microseconds) compare to singlet state (nanoseconds), the probability of interaction with other molecules is therefore higher, and the triplet state is subsequently often involved in photochemical reactions [45, 56, 61]. The excited triplet PS can undergo two different photochemical reations, defined as type I and type II [56].

Both type I and II reactions lead to ROS formation. ROS are capable to initiate a large number of reactions with biomolecules, including unsaturated lipids, amino acids residues in proteins like tryptophan and nucleic acid bases, particularly guanosine and guanine derivative [49, 61]. Type I and type II reactions can occur at the same time in PDT, however the ratio between these reactions is dependent on several factors including type of PS, amount of oxygen and substrate present [61, 63].

Type II reactions in PDT

Type II reactions are recognized as the most important mechanism for the biological effect in PDT [49]. In a type II reaction, there is a direct energy transfer to molecular oxygen, leading to the formation of molecular singlet oxygen [49]. According to the selection rule that constraint the possible transitions that can occur, only triplet-triplet interactions are allowed [44, 45].This means that the PS in triplet state can only interact with a molecule that also is triplet. Molecular oxygen is a triplet in its ground state and type II reactions are therefore favored in the prescence

of molecular oxygen [44, 45]. In this reaction the PS can be regenerated and can be involved in further cycles of excitation and generation of singlet oxygen as long as there is light exposure and sufficient amount of molecular oxygen present (figure 8) [61, 64].

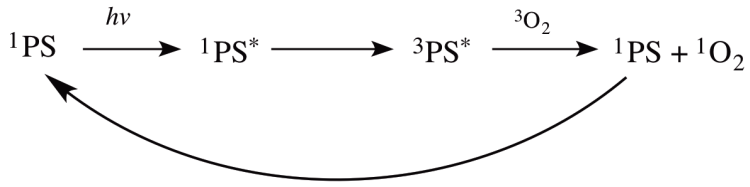

Figure 8 | **Regeneration of PS in a type II reaction.** *Hv*: light, ^1PS: photosensitizer at ground state, $^1PS^*$: photosensitizer at singlet state, $^3PS^*$: photosensitizer at triplet state, $^3O_2$: ground state oxygen, $^1O_2$: singlet oxygen. Adapted from Høgset *et al.* (2004) [64]

Type I reactions in PDT

Type I reactions involve the transfer of an electron or a hydrogen atom between the excited triplet PS and a substrate to produce radicals [49]. The electron transfer can proceed in either direction, usually the subtrate donates an electron to the PS leading to substrate radical cation and PS radical anion [65]. Both radicals may react with molecular oxygen which leads formation of cytotoxic ROS including superoxide anions ($O_2\cdot$-), hydroxyl radicals (OH·) and hydrogen peroxide (H_2O_2) [61]. In type I reactions, PS may not be available for regeneration since is it converted to an oxidized molecule (gain of electron) [65]. Type I reaction are favored in the absence of oxygen as oxygen compete with the other substrates for interaction with PS [65].

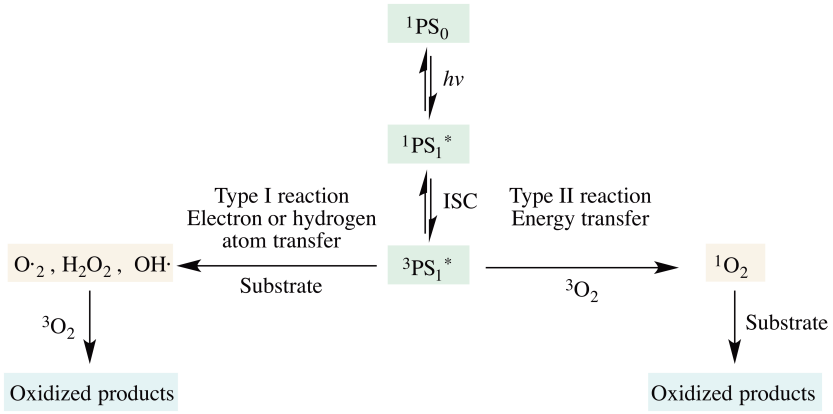

Figure 9 | **Type I and II reactions.** In type I reactions the excited PS reacts directly with a substrate. There is an electron or hydrogen atom transfer which produces radicals. In type II reactions, the excited PS transfers its excess energy to ground state molecular oxygen, which leads to production of singlet oxygen. Adapted from Oleinick (2010) [65]

1.4.3 PDT's effect on tumors

The extent of photodamage and cytotoxicity on a tumor following PDT is dependent on several factors, i.e. type of PS, extracellular and intracellular localization, PS dose, light dose, light fluence rate and oxygen availability [44]. PDT can mediate tumor destruction through three main mechanisms; direct cytotoxicity, vasculature damage and induction of immune response against tumor cells. These mechanisms can also influence on each other, however, it seems like a combination of all three mechanisms are required for long-term tumor control [44].

Direct cytotoxic effect

PDT induces a sequence of photochemical processes in the tumor cells. The cell subsequently attempts to repair the photodamage by, for instance, expression of antioxidants to counteract the effect of singlet oxygen and expression of heat shock proteins that protects the cell against stress [42]. The cellular function may in this way be restored, however, when the dose is sufficient PDT overwhelms the repair mechanisms. This leads to high level of ROS that induces direct cell death by apoptosis, autophagy or necrosis [42, 43, 66].

Apoptosis is the best-studied cell death pathway of all and is characterized by morphological changes involving nuclear condensation and general cellular shrinkage [66]. Necrosis is marked by cellular swelling and rapid loss of the plasma membrane integrity [66]. Necrosis is a major cell death pathway induced by PDT with PSs localized on the plasma membrane. This is likely due to a rapid loss of the intergrity and incapability to maintain ion fluxes across the plasma membrane [66].

Autophagy can also mediate cell death, which is a process where cytosol and organelles are encased in vacuoles, termed autophagosomes. When the autophagosome is fused with lysosomes, its content is digested and recycled [67]. Initially, autophagy was characterized as a survival response to a variety of stress conditions, for instance starvation and hypoxia. However, excessive and uncontrolled levels of autophagy induced by PDT has been defined as autophagic cell death [67]. The role of autophagy in the mechanisms of cell death following PDT is not completely understood. Furthermore, there is a considerable crosstalk between autophagy and the other death machineries [68, 69].

Vascular damage

In order for tumor cells to stay viable, they are dependent on oxygen and nutrients supplied by the blood vessels. Damage to the vascular cells may cause release of cytokines that results in platelet aggregration [42]. The accumulation of PS in vascular cells may induce shut down of the vascular and neovascular supply upon light exposure, and may subsequently deprive the tumor from oxygen and nutrients [44]. Photochemical induced damage of vasculature is the principle utilized for treatment of ADM with Visudyne® (section 1.4.1).

Induction of immune response

PDT was originally thought to be a local treatment at the site of illumination. However, it is now accepted that PDT also have a significant effect on the immune system [42]. Many studies have indicated that induction of necrosis is better at activating the immune system than apoptosis [70]. In apoptopic cells, the plasma membrane is intact with the cytosolic constituents isolated [70]. During necrosis, the cytosolic constituents are released locally into the extracellular space due to damaged plasma membrane [42, 70]. These potentially immunogenic constituents (antigens) can provoke a robust inflammatory response to generate an immune reaction against the tumor [42]. The PDT induced immune response is thought to consist of induction of inflammation and generation of long-term anti-tumor immunity [71]. PDT can induce acute inflammation, characteried by increased expression of several pro-inflammatory cytokines like interleukin 6 and tumor necrosis factor α [72]. It has been demonstrated that the degree of inflammation influences the anti-tumor immune response [72]. These acute inflammatory mediators attracts immune cells as neutrophils and dendritic cells (DCs). DCs can take up antigen, which leads to activation and maturation. Upon maturation, the DCs can present antigens to the T lymphocytes at the regional lymph nodes. Activated T lymphocytes become effetor T cells i.e. $CD8^+$ cytotoxic T cells. $CD8^+$ T cells are attracted by cytokines and migrate to the tumor to eliminate tumor cells [70]. Both pre-clinical and clinical studies have demonstrated that the efficacy of PDT is dependent upon $CD8^+$ T cells [72].

1.4.4 Light

Visible light is part of a much broader electromagnetic spectrum (fig. 10), and can be thought of as waves propagating through space. On the other hand, light can also behave as a particle, called a photon. Together these characteristics of light is termed “the dual nature of light” [45].

The energy of a single photon is described by $E_{photon} = hc/\lambda$, where h is Planck's constant (6.6×10^{-34} J s) , c is the speed of light in vacuum (3×10^{8} cm/s) and λ is the wavelength [45]. It is the energy from the photon that is absorbed when a molecule is excited, as in the exitation of a PS during PDT. In PDT *in vivo*, light from the red region of the spectrum is used as this has the ability to penetrate through the skin [73]. Wavelengths shorter than ~ 600 nm will be absorbed by the endogenous chromophores such as hemoglobin and melanin [28]. Using light with wavelength above 850 nm does not provide sufficient energy to generate triplet state of PS (fig. 10) [28].

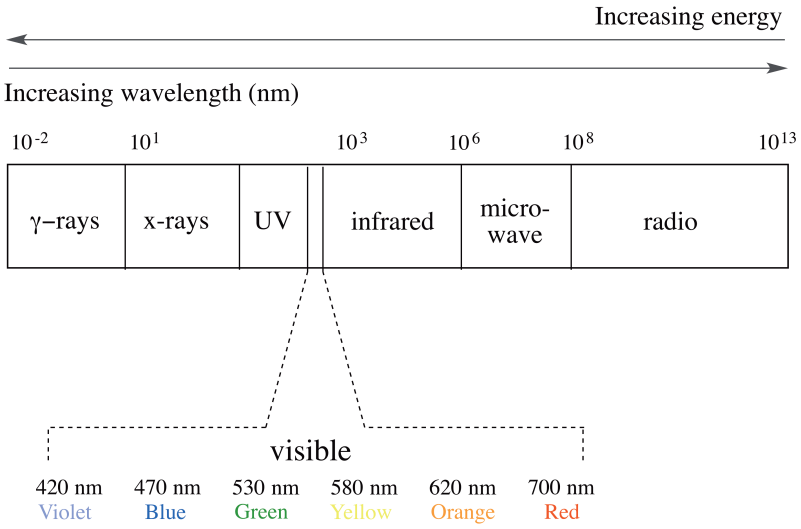

Figure 10 | **The electromagnetic spectrum with the visible region highlighted**. Adapted from Smith (2009) [74].

1.5 Photochemical Internalization (PCI)

Macromolecules with intracellular targets hold a great potential as novel cancer therapeutics, including DNA in gene therapy, gene silencing oligonucleotides and cancer vaccination with peptides and mRNA. Despite their potent activity, the intracellular delivery of macromolecules is severely limited by endocytosis unless they posess a mechanism for endosomal escape [75]. Macromolecules are taken up by endocytosis and are usually directed to lysosomes where they are enzymatically degradated [75]. In order to exert effect, the drug molecules must escape from the endosomes to reach their subcellular sites of action, often located in the cytoplasm or nucleus [75]. Failure to be released from endosomal compartments severely limits the efficacy. Lysosomal sequestration does not only apply to macromolecules, but also limits the efficacy of a variety of other currently approved cancer therapeutics (section 1.1).

Photochemical internalization (PCI) represents a treatment modality for release of drugs that accumulate in endosomes and lysosomes [64]. This is a method developed at the Norwegian Radium Hospital, and is based on the principle of PDT where it takes advantage of the photochemical effects induced by PS, light and oxygen [76]. In contrast to PDT, which relies on ROS-induced cytotoxicity to eradicate cancer cells, PCI utilizes the photochemical reactions for intracellular drug delivery [77]. PSs used in PCI are designed to specifically localize in the membrane of endocytic vesicles, and upon illumination rupture the vesicles for cytosolic drug release [1, 78]. As previously described, PSs have enhanced retention in tumor tissue compared to normal tissues (section 1.4.1). This makes PCI an attractive drug delivery system for cancer therapeutics. The light can be site-directed and hence only tissue subjected to light will have the drug delivered. Toxicity in normal tissue can be prevented due to reduced accumulation of PS [1]. It has previously been demonstrated that PCI have the ability induce deeper tumor necrosis and larger vascular effect compared to PDT with the same PS and same light dose [79-81].

PCI has a wide application area and the use of this tecnology has been documented for various macromolecules and drugs *in vitro* including proteins, genes carried by non-viral and viral vectors, petide nucleic acids, nanoparticles, siRNA and some chemotherapeutic agents [76]. Reversal of drug resistance of the chemotherapeutic doxorubicin has been demonstrated in MDR breast cancer cells. Doxorubicin was here lysosomal sequestered and PCI induced a doxorubicin sensitivity in resistant cells to a comparable level as observed in parental cells [16, 82]. The principle of PCI has been demonstrated in more than 80 different cells lines and also in more than 10 different xenograft models of various cancers in mice [76].

"Light first" and "light after" strategy

The standard procedure *in vitro* for PCI includes incubation of PS and the drug of interest prior to light exposure ("light after"-procedure), however it is also possible to incubate the drug after the photochemical reaction termed "light first"-procedure (fig. 11). The "light first"-procedure was first demonstrated *in vitro* using gelonin, a ribosomal inactivating protein toxin, and transfecting nucleic acids [83]. This strategy was indicated as at least as efficient as the standard "light after" procedure. The *in vivo* effect of "light first"-procedure was later confirmed in BALbc nu/nu mice with subcutaneous human colorectal adenocarcinoma tumors with gelonin administered immediately after light exposure [84]. The exact cellular mechanism behind the

"light first"-procedure is not known, but a possible mechanism is fusion between the photochemically ruptured vesicles and intact vesicles carrying the drug, leading to endosomal release into the cytosol (fig. 11) [83].

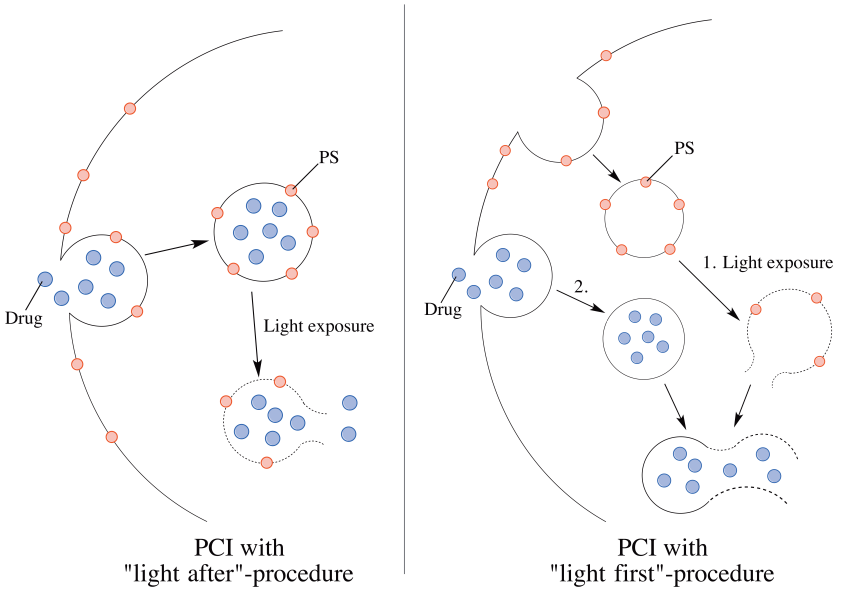

Figure 11 | "**Light first"- and "light after"-procedure**. In the "light first"-procedure PS and light is given before the drug. This leads to fusion of ruptured and intact vesicle with drugs, thus endosomal release into the cytosol. With the "light after"-procedure, both PS and drug are given before light exposure. Upon photochemical reaction the vesicles rupture and release its content into the cytosol. Adapted from Berg *et al.* (2006) [84].

1.5.1 PSs in PCI

The PSs used for PCI are amphiphilic and can reside at the membrane without fully crossing into the cytosol [77]. The hydrophobic part of the PS associates with the cell membrane whereas the hydrophilic part faces the extracellular space. When the PS is endocytosed by adsorptive endocytosis, the vesicle wall will be lined with PS [77]. The most common PSs for PCI are $AlPcS_{2a}$ (aluminium phatlocyanine disulfonate), $TPPS_{2a}$ (meso-tetraphenyl porphyrin disulphonate) and $TPCS_{2a}$ (meso-tetraphenyl chlorin disulphonate) [1, 84]. These PSs are based on the porphyrin/chlorin structure and have two sulphonate groups on adjacent phenyl rings which give the amphiphilicity neccesary (fig. 12). At physiological pH, the two sulphonate groups will remain permanently ionized while the core is uncharged [85].

$AlPcS_{2a}$ contains coordinated diamagnetic metal ion, aluminium (fig. 12). Most PSs lack coordinated metal ions as this decreases its lifetime of triplet state and subsequently the ability to produce singlet oxygen [47]. However metal PSs have been developed as they have improved

solubility and stability [47]. Preclinical evaluation of PCI performed with $AlPcS_{2a}$ showed that this is not an optimal PS for clinical use due to large numbers of isomers which can potentially lead to batch-to-bacth variations. The PS $TPCS_{2a}$ was therefore developed for clinical utilization of PCI where $TPCS_{2a}$ is synthesized from $TPPS_{2a}$ by di-imide reduction [86]. $TPCS_{2a}$, now marketed as Amphinex® (PCI Biotech AS), was found to be clinically suitable for PCI and is used in clinical trials [87].

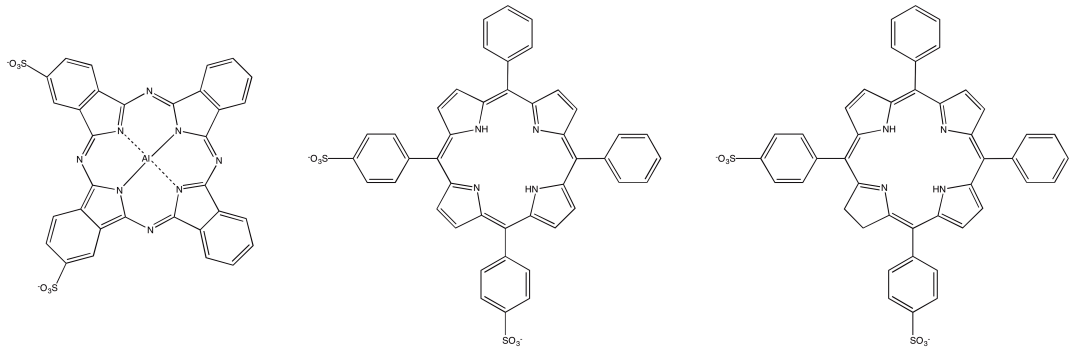

$AlPcS_{2a}$ $TPPS_{2a}$ $TPCS_{2a}$

Figure 12 | **Chemical structures of PSs used for PCI.** $AlPcS_{2a}$: aluminium phatlocyanine disulfonate, $TPPS_{2a}$: meso-tetraphenyl porphyrin disulphonate, $TPCS_{2a}$: meso-tetraphenyl chlorin disulphonate. Adapted from Berg *et al.* (2011 and 2010) [78, 87]

1.5.2 Ribosome-inactivating proteins (RIPs) and PCI

PCI in combination with type I RIPs has been documented both *in vivo* and *in vitro* [76]. RIPs arrest the protein synthesis by acting on the ribosomes (N-glycosidase activity) leading to cell death [88]. Both type I and type II RIPs have the enzymatically active chain that is responsible for the ribosome-inactivation. This chain is approximately 30kDa [76]. However type II RIPs also have a cell-binding chain that binds to cell surface receptors, mediate cellular uptake and translocation to cytosol. The absence of a cell-binding chain in type I RIPs limits the entry thus the toxicity [76]. However, type I and II RIPs have similar toxicity once they are translocated to cytosol. Ricin is an example of type II RIPs, and gelonin and saporin a type I RIPs. Type I RIPs are good candidate for PCI, and PCI has been shown to improve the delivery of both gelonin and saporin [76]. Furthermore, type I RIPs coupled with targeting moieties have been explored with PCI and have shown to improve cytotoxicity compared to non-coupled RIPs [76, 80].

1.5.3 Clinical application of PCI

Based on pre-clinical experiments, PCI is a promising strategy against many types of cancer. In 2009-2011, the first PCI-based clinical trial (ClinicalTrials.gov identifier: NCT00993512) was carried out using Amphinex® ($TPCS_{2a}$) and the cytostatic drug bleomycin. This was a phase 1, dose-escalating study in patients with local recurrence or advanced/metastatic, cutaneous or sub-cutaneous malignancies. Three different dose levels of Amphinex® and fixed dose of bleomycin were used. The preliminary efficacy data of Amphinex®-based PCI of bleomycin was found to be encouraging, and well tolerated in these patients [89]. An extension study was later carried out in 2012-2013 to observe whether lower doses of Amphinex® than the initial study dose (0,25 mg/kg) in PCI with bleomycin would give comparable or improved efficacy (ClinicalTrials.gov identifier: NCT01872923). Currently, a phase I/II Amphinex®-based PCI study is recruiting participants (ClinicalTrials.gov identifier: NCT01900158). This is a dose escalation study that will assess the safety, tolerability and efficacy in PCI of gemcitabine followed by administration of gemcitabin/cisplatin chemotherapy in patients with chloangiocarcinomas.

2 Materials and methods

2.1 Cell lines and cultivation

The human colorectal adenocarcinoma cell line HT-29 (ATCC® HT-38™) was used as a research model in this study. HT-29 cells were purchased from the American Type Culture Collection (ATCC, Manassas, Va., USA). This cell line expresses VEGFR [90]. HT-29 was maintained in McCoy's 5a Medium (ATCC® 30-2007™), as recommended by ATCC [10], supplemented with 100 IU/ml penicillin (Sigma-Aldrich, St. Louis, Mo., USA), 100 µg/ml streptomycin (Sigma-Aldrich) and 10 % fetal bovine serum (Thermo Fisher Scientific, Waltham, WA, USA, Lot. No. 41G3930K) in a humidified incubator containing 5 % CO_2 at 37 °C.

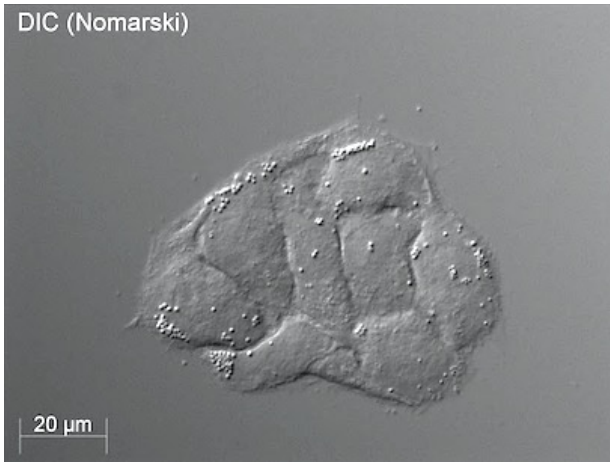

Figure 13 | **Morphology of HT-29.** Image of a colony of HT-29 cells. 63x magnification. Scale bar = 20 µm.

The cells were cultured in 75 cm^2 and 175 cm^2 Nunc™ Cell Culture Treated EasYFlasks™ (Thermo Fisher Scientific). Aseptic procedures were used in all experiments involving cells using a laminar flow hood.

Production of the sunitinib resistant cell line: HT-29/SR

Sunitinib-resistant cell lines of HT-29 have previously been established by Dr. Anette Weyergang and Dr. Maria Elisabeth Brandal Berstad, and cryopreserved in the PCI group at the Norwegian Radium Hospital. There were however, viability problems associated with the cryogenic storage and a new sunitinib resistant cell line, HT-29/SR, had to be produced. To induce resistance, parental HT-29 cancer cells were continuously exposed to 2 µM sunitinib.

Sunitinib was added directly in the culture medium. Sunitinib malate (Cat. No. PZ0012) purchased from Sigma-Aldrich (St. Louis, Mo., USA), was provided as a powder and dissolved in 100 % DMSO to make stock solutions of 2,5 mM and 14,27 mM. Aliquots of sunitinib were made to avoid numerous freeze-thaw, and the solutions were stored at -20 °C. Each aliquot did not undergo more than two freeze-thaw cycles. Untreated parental HT-29, herinafter referred to as HT-29/PAR, cells were kept alongside the sunitinib-treated cells as a control. Experiments were initiated after 1 month of sunitinib exposure. A decreased sensitivity to sunitinib was then detected by the MTT assay, where HT-29/PAR and HT-29/SR cells were exposed to different sunitinib concentrations to assess sunitinib senstivity (section 3.2.2). HT-29/SR cells were continuously kept on sunitinib throughtout the current thesis ~ 5 months and the resistance was found to be persistent.

2.2 Standard procedures

2.2.1 Subcultivation

Both HT-29/PAR and HT-29/SR were subcultured 2-3 times per week and never allowed to grow confluent. HT-29/PAR cells were subcultured at a ratio between 1:5 and 1:8. HT-29/SR was subculture at a ratio between 1:4 and 1:6.

Procedure

- Used culture medium was carefully removed from culture flask.
- 3-5 ml preheated phosphate buffered saline (PBS) without calcium and magnesium (Sigma-Aldrich, Cat. No. D8537) was added, and the cells were briefly rinsed. This step was included to fully remove serum which inhibits trypsin.
- PBS was removed, and 2-3 ml preheated trypsip-EDTA solution (Sigma-Aldrich, Cat. No. T3924) was added. Trypsin has protease activity and disturbs the cell-cell interactions and cell-substratum interactions, which allows the cells to dettach from the flask. Trypsin has an optimal temperature of 37 °C, and the culture flask was therefore placed in an incubator for 1-3 minutes.
- The culture flask was observed under microscope and gently tapped to allow remaining attached cells to be released.

- 10 ml of culture medium was added once all the cells were deattached to inhibit trypsin activity. Prolonged trypsin exposure can damage cell surface. The required fraction of cell suspension was transferred to a new labelled culture flask containing pre-heated culture medium. 18 ml and 42 ml culture medium for 75 cm^2 and 175 cm^2 flasks, respectively.

2.2.2 Cryopreservation

Seed stocks of both HT-29/PAR and HT-29/SR were made during this thesis. The cells were cryopreserved at 2, 3 and 5 months after production of resistant HT-29 cells. Freezing medium was prepared before trypsinating cells. The freezing medium consisted of 40 % culture medium, 50 % fetal bovine serum and 10 % DMSO from Sigma-Aldrich (Cat. No. D8418). DMSO is a cryoprotectant that reduces the freezing point of the medium and allow slower cooling rate which reduces the risk of ice crystal formation. Ice crystals can damage cells and cause cell death.

Procedure

- The cells were trypsinated (according to section 2.2.1), added excess of culture medium and centrifuged for 3 minutes at room temperature to pellet cells.
- Supernatant was carefully removed without disturbing the cells.
- Freezing medium was added dropwise over 2 minutes and cell pellet resuspended.
- Cell suspension was aliquoted into pre-labelled cryogenic vials (Nunc® CryoTubes®, Sigma-Aldrich). Cryogenic vials were inserted in Mr Frosty™ Freezing Container (Sigma-Aldrich). Mr. Frosty™ contains slots for cryogenic vials and is a system designed to achieve a rate of cooling close to -1°C/minute, which is the optimal rate for cell preservation. The container was transferred to a – 80 °C freezer and stored overnight.
- The vials were then moved to a nitrogen freezer for prolonged storage.

2.2.3 Thawing and propagation of cells

Procedure

- Cryogenic vials from nitrogen freezer were thawed rapidly (< 1 minute) in a 37 °C water bath.
- 5 ml of pre-heated culture medium was added dropwise to dilute thawed cells.
- The cells were then centrifuged for 3 minutes at room temperature to remove any traces of DMSO, which is toxic to cells.
- The supernatant was carefully removed and cell pellet resuspended with 5 ml culture medium.
- Cell suspension was transferred to a labelled 175 cm^2 flask with 42 ml pre-heated culture medium. The culture medium was changed the next day or was subcultured if necessary. After a week, the cells were used for experiments.

2.2.4 Cell counting

The number of cells in a suspension was counted using Glasstic® Slide from KOVA with hemocytometer counting grid (Cat. No. 87144/87144E, Garden Grove, CA, USA). 10 µl of the cell suspension was transferred to the hematocytometer chamber and observed under microscope. The grid contains nine squares. Three of the squares in diagonal were counted and an average was found. The volum of one square is 0,1 µl and the average was multiplied with 10^4 to obtain the number of cells/ml. Based on this, number of cells to seed out for experiments could be determined using following formula: $c_1 v_{1=} c_2 v_2$ where

c_1 is the initial number of cells/ml in cell suspension
v_1 is the volume (ml) needed to from the cell suspension
c_2 is the desired number of cells/ml for experiment
v_2 is the desired end volume (ml)

2.3 PDT- and PCI-treatment of cells

2.3.1 Light source and PS

$TPCS_{2a}$ (0,35 mg/ml, Amphinex®) was provided by PCI Biotech AS (Oslo, Norway) and stored at 4 °C, protected from light. All work with $TPCS_{2a}$ was performed under subdued light. PDT and PCI experiments were performed with red diode lamp and LumiSource™ blue lamp. LumiSource™ delivers light with highest fluence around 435 nm (fig. 15) with a fluence rate of 11,7 mW/cm^2 [91]. It consists of four light tubes (Osram 18W/67) [91]. The red lamp delivers light at 650-660 mm wavelength with a fluence rate of $6mW/cm^2$. The lamps were turned on at least 15 minutes before illumination to ensure that the light intensity was homogeneous and stable over time.

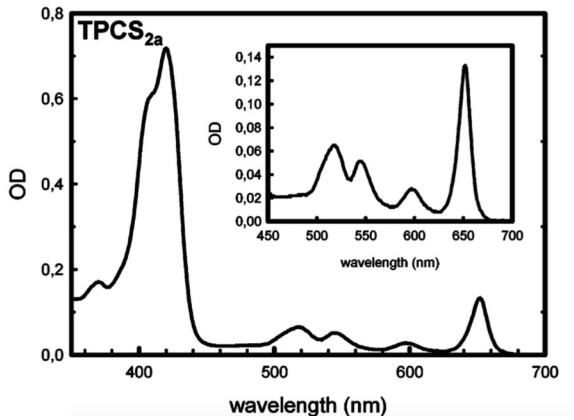

Figure 14 | **Absorption spectrum of $TPCS_{2a}$ dissolved in 10 % Cremophor ELP.** Both graphs show the absorption peaks of $TPCS_{2a}$. The inset is a magnification of the peak in the red region (~ 650-700 nm). Modified figure from Berg *et. al* (2011) [86]

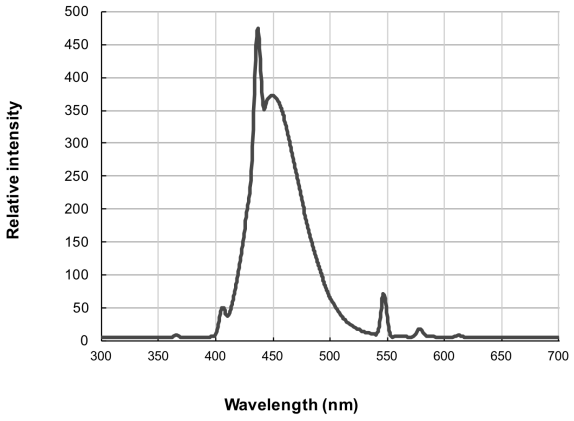

Figure 15 | **Emission spectrum of LumiSource™.** Graph provided by Kristian Berg.

2.3.2 PDT and PCI *in vitro*

PDT and PCI experiments were carried out in 96 well-plates (Nunc 96 MicroWell® with Nunclon® Delta Surface, Thermo Fisher Scientific) and 6-well plates (6-well multidish Nunclon® Delta Surface, Thermo Fisher Scientific). The cells were seeded out 4-5000 cells/well for 96 well-plates and 500 cells/well for 6 well-plates, and placed in an incubator for attachment. In all PDT and PCI experiments, attached cells were incubated 18 hours with 0,4 µg/ml $TPCS_{2a}$, washed twice with PBS and chased 4 hours in a drug-free culture medium prior to illumination with indicated lamp and exposure time. This is the standard PDT protocol. Cytotoxicity was assessed with the MTT (96-well plates) or clonogenic assay (6-well plates).

PCI using the "light after"-procedure with recombinant toxin gelonin (rGel), genereously provided by Dr. Michael Rosenblum's laboratory at M.D. Anderson Cancer Center (Houston, TX, USA), was performed according to the standard PDT protocol but with co-incubation of $TPCS_{2a}$ and rGel at indicated concentrations. Initally, the cells were incubated with rGel 4 hours, during chase, but this was later changed to an 18 hours co-incubation with $TPCS_{2a}$. Aliquots of rGel, 1mg/ml and 5,34 mg/ml, were stored in a -20 °C freezer. In "light after"-procedure with sunitinib, the cells were initially co-incubated 18 hours with $TPCS_{2a}$. This procedure was later changed to incubation with sunitinib at indicated concentrations for 48 hours prior to a 18 hours co-incubation with sunitinib and $TPCS_{2a}$. The cells were then washed, chased and exposed to light according to the standard PDT protocol. The "light first" protocol was only performed with sunitinib where the standard PDT protocol was followed by an immediate administration of sunitinib. Sunitinib incubation was sustained until the end of the experiment.

2.4 Assays for cytotoxicity and viability measurements

2.4.1 The MTT cell viability assay

The MTT (3-(4,5-dimethylthiazol-2-yl)-2,5-diphenyltetrazolium bromide) assay is used to measure the viability of cells. The reagent is positively charged and can penetrate viable eukaryotic cells. Mitochondrial enzymes reduce the reagent resulting in the formation of insoluble purple formazan crystals [92]. These crystals can be solubilized by DMSO and the

color of the solution can then be measured spectrophotometrically. MTT (Cat. No. M2128) from Sigma-Aldrich was provided as powder. MTT was dissolved in PBS to a stock solution of 5 mg/ml, sterile filtered and stored at 4 °C, protected from light. Initially, 4 hours incubation with MTT 0,25 mg/ml was used on the cells. However, due to problems with dettaching cells the procedure was changed to 0,5 mg/ml MTT and 30 minutes incubation time. Viability was assessed 48-96 hours post light exposure or drug incubation as indicated in the result part.

Procedure

- Used culture medium was removed, and MTT in culture medium was added to the wells. MTT was also added to an empty row on the plate to serve as blank in order to eliminate background absorbance.
- The plate was incubated for 30 minutes and examined under microscope for sufficient amount of purple formazan crystals, and to ensure that no cells were dettaching.
- Culture medium was carefully aspirated, leaving the formazan crystals in the wells.
- 100 µl DMSO was added to each well, including blank wells.
- The plate was placed in a a titer plate shaker for 5-10 minutes. When all the crystals were dissolved, the plate was analyzed by PowerWave™ XS2 Microplate Spectrophotometer (BioTek Instruments, Inc.,Winooski,VT, USA). The optical density was measured at 570 nm, and the results were analyzed using Gen5™ Data Analysis Software (BioTek Instruments, Inc.).

2.4.2 Clonogenic assay

The clonogenic assay is regarded as the gold standard for *in vitro* measurements of cytotoxicity [93]. This assay determines the long-term effects of a treatment and evaluates the cells ability to form colonies. A low number of cells are plated out to allow colony formation. It is assumed that each colony is derived from a single cell. When visible colonies are formed, they can be fixated and stained with methylene blue. Based on colony count, cell survival can be estimated [94]. The clonogenic assay was here performed in 6-well plates.

Procedure

- Cells were seeded (500 cells per well) and allowed to attach for 24 hours.

- After 24 hours, the cells were subjected to indicated treatment. Following treatment the medium was refreshed if necessary over a period of 10-14 days. Colonies were fixed and stained when suffiently large colonies (> 50 cells/colony) were formed in the controls, estimated by microscopy.
- Fixation and staining were performed outside the laminar flow hood. Culture medium was removed and 1 ml NaCl solution 0,9% was added to each well.
- The NaCl solution was then removed and 1 ml absolute ethanol (VWR Corporation, Radnor, PA, USA, Cat. No. 20821.310DP) was added to each well. The colonies were fixated with absolute ethanol,10 minutes at room temperature.
- Absolute ethanol was then removed and 1 ml unsaturated methylene blue was added to each well for 5 minutes.
- The methylene blue was removed and the plates were carefully immersed in a pan with tap water to remove any excess of color before counting
- When the plates had air-dried, colonies were manually counted using an automatic E-Count™ colony counter pen (Heathrow Scientific, Vernon Hills, IL, USA) under a magnifying glass.
-

Parameters that were determined by clonogenic assay were the plating effieciency (PE) and the surviving fraction (SF) that were calculated with following formulas:

$$\text{PE } \% = \left(\frac{\text{number of colonies formed}}{\text{number of cells seeded}}\right) \times 100\%$$

$$\text{SF } \% = \left(\frac{\text{number of colonies formed after treatment}}{(\text{number of cells seeded} \times \text{PE})}\right) \times 100\%$$

2.4.3 IncuCyte® ZOOM live-cell analysis

IncuCyte® ZOOM system enables observation of cell behaviour over time by gathering and analyzing phase-contrast images at defined time intervals. A microscope is inserted inside a cell incubator, and a networked external controller hard drive gathers and processed the image data. 96-well plates were used in all IncuCyte® ZOOM experiments and cell proliferation was monitored by analyzing the occupied area (% confluence) of cell images over time. Increasing confluence was therefore a surrogate for proliferation. IncuCyte® ZOOM was used to generate growth curves and calculate doubling times in HT-29/PAR and HT-29/SR. The cells were

seeded out and immediately placed in an incubator connected to the IncuCyte® ZOOM system. The image acquisition time was set every three hour with one image aquired per well. The cells were monitored and observed by looking at image data. Fresh culture medium was added to the wells if necessary, without disturbing the cells. The plates were examined visually during the experiment, and if half of the medium had evaporated from the wells, 50 µl of fresh medium was added directly into each wells.

2.5 Fluorescence detection

Fluorescence is emission that results from absorption of photon (fig. 7). The fluorescent effect is used in a number of spectroscopy techniques including fluorescence microscopy and flow cytometry. A sample is treated with fluorescent reagent where these reagents are able to absorb light at cetain wavelength and emit light at longer shifted toward the red end of the spectrum from the absorbed light. Each fluorescent reagent exhibits its characteristic absoprtion and emission spectra depending on the chemical structure.

2.5.1 Fluorescence microscopy

The fluorescence reagent in a sample can be selectively examined by manipulation of the excitation light and emission light using filters. The filters allow light of required wavelengths to pass and block other light as completely as possible (fig. 16). A fluorescence microscope also contains a dichroic mirror that splits the light into different wavelengths and only transmits the longer wavelength (fig. 16).

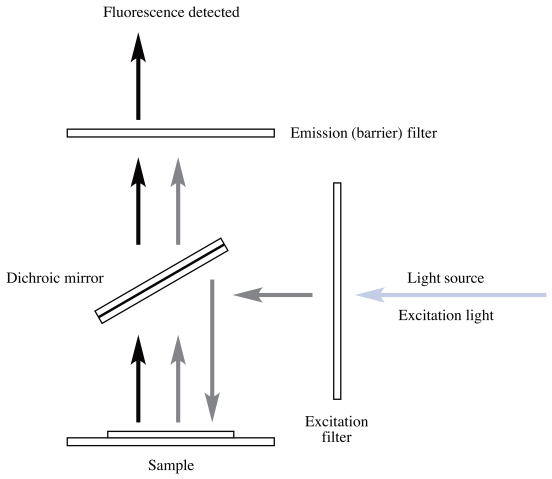

Figure 16 | **Arrangement of filters and light source in a fluorescence microscope.**

Fluorescence microscopy was used to visualize the subcellular location of sunitinib and $TPCS_{2a}$ in both HT-29/PAR and HT-29/SR. 48 wells plate with Nunclon® Delta Surface (Sigma-Aldrich) were used for fluorescence microscopy experiments.

Before plating, one round coverslip of glass (10 mm diameter) was added in each well. The cells were trypsinated and 30 000 cells per well was plated (section 2.2.4 and 2.3.2) and placed in an incubator for attachment. The cells were incubated in fluorescent agent-free medium for 24 hours. Non-treated cells were also included in each experiment to eliminate autofluorescence as fluorescence detection can be compromised by background signals. The fluorescent reagents were added directly into the well and the following were used:

Sunitinib

The cells were incubated 24 hours with 2 µM sunitinib. Sunitinib has a maximum absorbance at 429-430 nm, and flourescence maximum at 540 nm (fig. 17 and fig. 23) [95].

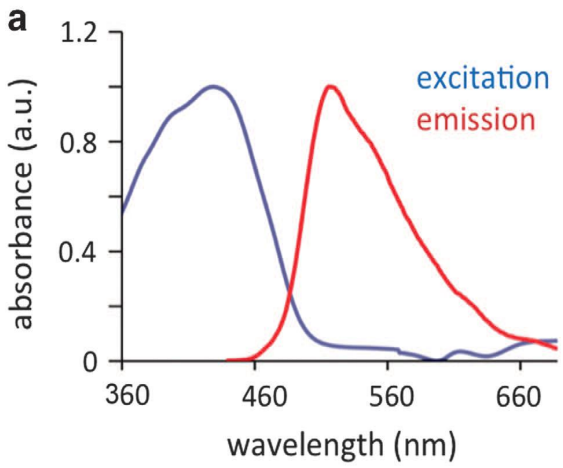

Figure 17 | **Spectral properties of sunitinib.** Figure from Nowak-Sliwinska et al. (2015) [95]

$TPCS_{2a}$

The cells were incubated 18 hours with 0,4 µg/ml $TPCS_{2a}$, followed by wash with PBS twice and 2 hours chase before image acquisition. The absorption spectrum of $TPCS_{2a}$ can be found in section 2.3.1. $TPCS_{2a}$ has a absorption maximum at 415 nm and 652 nm (fig. 14) [86, 87]. The fluoresence emission of $TPCS_{2a}$ have two distinct maxima at 656 nm and 725 nm (fig 18) [87].

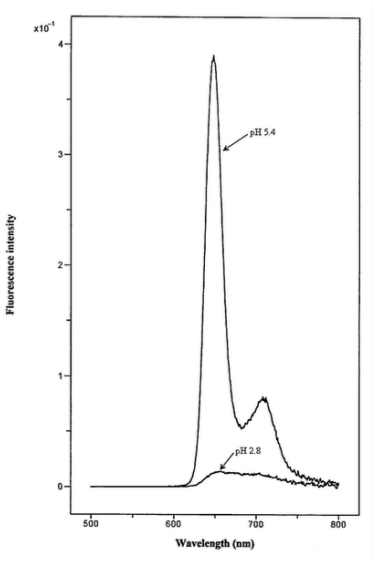

Figure 18 | **Emission spectrum of $TPCS_{2a}$. Figure** from Lilletvedt *et. al.* (2011) [85]

Hoechst 33342

Hoehcst 33342 was purchased from Thermo Fisher Scientific (Cat. No. 62249). Hoechst 33342 is a nucleic acid stain. Stock solutions were in 10 mg/ml and aliquots were stored at 4 ºC, protected from light. Working concentration was 100 µM and incubation time 15 minutes prior to image acquisition. Hoechst 33342 has a maximum excitation at 350 nm and emission at 461 nm (fig. 19).

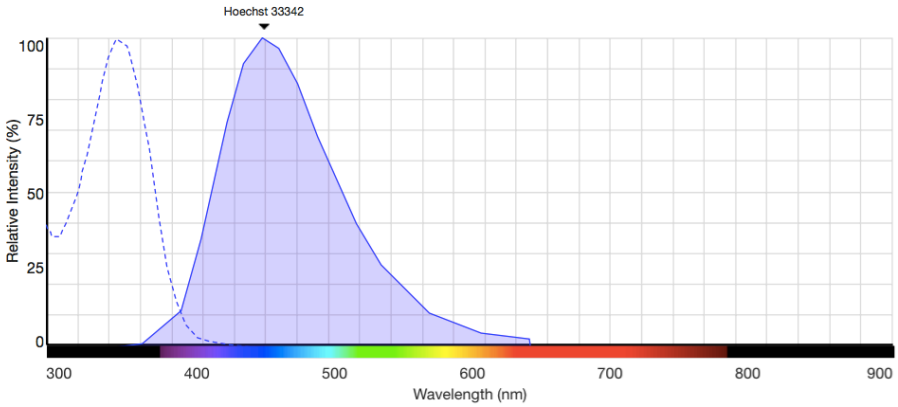

Figure 19 | **Spectral properties of Hoechst 33342.** Figure from Fluorescence SpectraViewer at https://www.thermofisher.com/

LysoTracker® Red DND-99 and LysoTracker® Green DND-26

LysoTracker® Red DND-99 and Green DND-26 were purchased from Thermo-Fischer Scientific (Cat. No. L7528 and L7526 respectively). LysoTrackers® were used to track acidic organelles in live cells, for example lysosomes. Stock concentrations of 1mM in aliqouts were stored at - 20 ºC, protected from light. The working concentration was 75 nM and the incubation time 30 minutes prior to image aquisition. LysoTracker® Red DND-99 has maximum excitation and emission at 577 nm and 590 nm, respectively (fig. 20). LysoTracker® Green DND-26 has maximum excitation at 504 nm and emission at 511 nm (fig. 19).

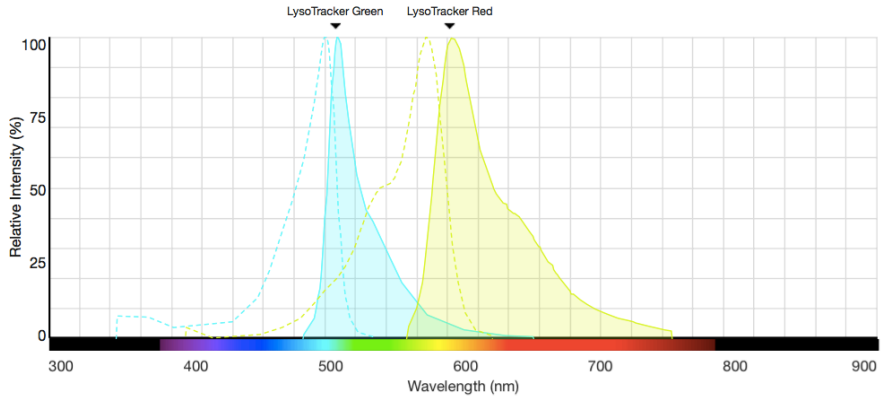

Figure 20 | **Spectral properties of LysoTracker® Red and Green.** Figure from Fluorescence SpectraViewer at https://www.thermofisher.com/

In separate experiments the following combinations were used:

- Sunitinib, LysoTracker® Red DND-99 and Hoechst 33342
- $TPCS_{2a}$, LysoTracker® Green DND-26 and Hoechst 33342

Before image acquisition the coverslips were carefully removed from the wells and submerged in ice-cold PBS twice. Excess PBS was removed and flipped on a microscope slide. A small drop of immersion oil was added on top of the coverslip. Images were aquired with appropriate optical filters on an Axioplan fluorescence microscope (Carl Zeiss AG, Oberkochen, Germany) using an objective with 63x magnification. The flourescence was detected by a AxioCamMR3 camera (Carl Zeiss). The microscope software AxiocVision Analysis (Carl Zeiss) was used to process and analyzed the fluorescence images. Filter settings used during image acquisition can be found in table 1. Both positive and negative controls were included in all experiments to avoid overlap of fluorescence signals. Positive controls contained only one fluorescent agent

and were checked against all the optical filters. Fluorescence images that were used for comparison were adjusted to the same display (brightness, gamma and contrast).

Fluorescencent agent	Excitation filter	Emission filter
Sunitinib	495 nm	519 nm
$TPCS_{2a}$	431 nm	545 nm
LysoTracker® Red DND-99	595 nm	620 nm
LysoTracker® Green DND-26	495 nm	519 nm
Hoechst 33342	359 nm	461 nm

Table 1 | **Filter settings used during image acquisition.**

2.5.2 Super-resolution microscopy

Super-resolution microscopy allows image acquisition with a higher resolution than fluorescence microscopy. This was performed to examine the intracellular co-localization of sunitinib and $TPCS_{2a}$. Images were acquired using a DeltaVision OMX V4™ Blaze 3D-SIM Super-resolution microscope from Applied Precision/GE Healthcare (Litle Chalfont, UK). Image acquisition was performed and analyzed by Dr. Vigdis Sørensen from the Superresolution Microscopy Core Facility at the Norwegian Radium Hospital. These experiments were only performed in the HT-29/SR cell line.

Procedure

- 300 000 cells/ml were seeded out in glass bottom dishes (Cat. No. P35GC-1.5-10-C) from MatTek Corporation (Ashland, MA, USA) and placed in an incubator 24 hours for attachment.
- Sunitinib and $TPCS_{2a}$ were added directly into the dishes to a final concentration of 2 μM and 0,4 μg/ml respectively, and incubated for 18 hours.
- The dishes were washed twice with PBS and chased 2 hours in serum-free FluoroBrite™ DMEM from Thermo Fisher Scientific (Cat. No. A1896701). This is a color-less culture medium used for fluorescence signal enhancement.

- Trolox from Sigma-Aldrich (Cat. No. 238813) was added directly into the dishes 15 minutes before image acquisition to a final concentration of 2 mM. Trolox is an anti-fade reagent that reduces photobleaching during live cell imaging. Trolox comes in powder and was dissolved in ethanol to 100 mM stock concentration stored at -20 °C.

2.5.3 Flow cytometry

Flow cytometry is a technique that detects scattered light and fluorescence of a cell as it flows in a fluid stream through a beam of light. This can be used to measure cellular size and relative fluorescence intensisty. A flow cytometer is made of three main systems: fluidics, optics and electronics [96]. The fluidics system delivers cells from cell suspention in a stream to the laser beam for interrogation. The portion of fluid stream where cells are located is called sample core. The width of sample core can be manipulated, in this study the width was restricted so that cells could pass through one by one [97]. The optics system consists of lasers that illuminate the cells in the sample stream and optical filters that gather and direct the light to appropriate detectors. Detected signals are converted into electronic signals by the electronics system for processing [96]. Light is scattered as the cells enters the sample stream and factors that contribute to light scattering are size, granularity and structural complexity inside the cell. Forward-scattered light (FSC) is proportional to cell size. Side-scattered light (SSC) is caused by granularity and internal complexity as well as fluorescence [96].

In these experiments, sunitinib fluorescence was detected by SSC which is proportional to flourescence intensity [97]. Flow cytometry was performed on both HT-29/PAR and HT-29/SR cells. Violet laser (405 nm) was used to excite sunitinib where following filter settting was used: band/pass 585/42 (543 nm-627nm) and long pass 545 nm. Flow cytometry was perfomed with a BD™ LSR II flow cytometer (BD Company, Franklin Lakes, NJ, USA) with the help of Ph. D. candidate Cathrine E. Olsen.

Procedure

- The cells were seeded out in 6-well plates (150 000 cells/ml) and placed 48 hours in an incubator with drug-free medium.
- After 48 hours, sunitinib was added directly into the well to a final concenration of 2 μM and incubated for 24 hours.

- The cells were trypsinated (section 2.2.1) using 500 µl PBS and trypsin for each well, and 2 ml culture medium to inhibit trypsin activity. The cell suspension was centrifuged for 3 minutes at room temperature.
- Supernatant was carefully removed and the cell pellet was resuspended with 500 µl pre-heated PBS. The cell suspension was transferred to a flow tube, and data were analyzed with the software programs BD FASCDiva Software (BD Company) and FlowJo (Three Stars Inc., Ashland, VA, USA).

2.6 Absorption and emission spectra

Sunitinib stock solution of 2,5 mM was diluted with DMSO to 30 µM. Sample preparation was carried out in subdued light. The sunitinib solution was transferred to a quartz cuvette (Cat. No. 104-10-40) from Hellma Analytics (Müllheim, Germany) where both absorbance and fluorescence were measured. Absorption and emission spectra was recorded at room temperature. For aborbance measurements, a cuvette with DMSO only was used to eliminate background. UV-visible absorption spectra (300-750 nm) were recorded by a Shimadzu (Kyoto, Japan) UV-2550PC spectrophotometer. Acquired data were analyzed using the software UVProbe. Emission spectrum was generated based on fluorescence measurements from a Cary Eclipce Fluorescence Spectrophotometer (Varian Inc., Palo Alto, CA, USA). The data were analyzed with the software program Cary Eclipse Scan Application.

2.7 Data analysis

Data are expressed as means ± SD unless otherwise described. When appropriate, the results are shown as normalized data (percentage of control). Graphs were generated using the scientific data analysis and graphing software SigmaPlot™version 12.5 (Systat Software Inc., San Jose, CA, USA). Statistical analysis was carried out using two-sided *t* test in SigmaStat™, and a value $p < 0,05$ was considered statistically significant. All the experiments have been reproduced three times, unless otherwise described.

3 Results

3.1 Growth curves and doubling times

Growth curves were established to determine the number of cells to be seeded in each experiments (fig. 21). It is important that the cells do not reach confluency and are in the log-phase during the experiments.

3.1.1 Growth curve of HT-29/PAR cells

At confluency (> 80%), cells have decreased growth rate which may affect the experiment results. HT-29/PAR cells were seeded out in 96-well plate at increasing density, ranging from 2000 to 12000 cells per well, and observed with IncuCyte® (procedure 2.4.3).

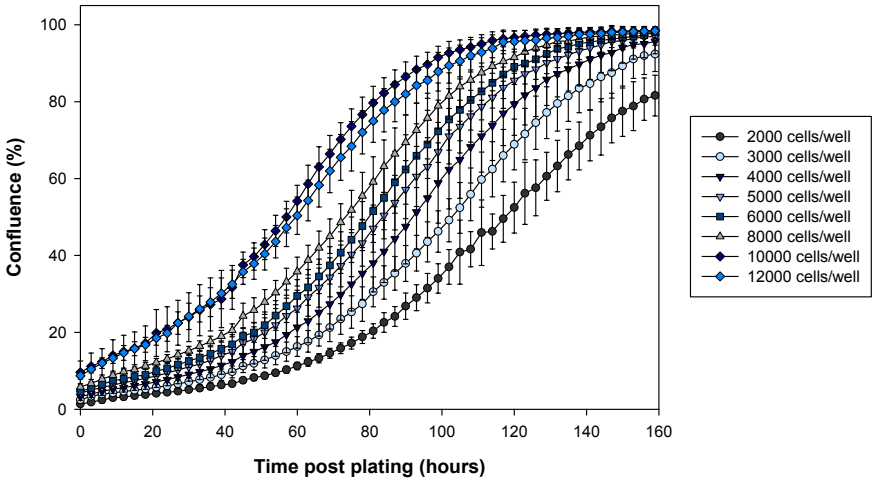

Figure 21 | **Growth curve of HT-29/PAR.** Cells were seeded at increasing density and observed by IncuCyte®. Representative results from one experiment. Each point is the average of 6 wells.

Most of the PCI and PDT experiments were performed in 96-well plates over a period of 116 hours or 140 hours from plating of cells to the end of experiment. Based on the growth curves (fig. 21), 5000 and 4000 cells per well were used in experiments lasting for 116 hours and 140 hours, respectively. This seeding density ensured that the cells were in the log-phase and did not reach confluency (plateau) during the experiments.

3.1.2 Population doubling time of HT-29/PAR cells

Based on the data from IncuCyte®, the population doubling time (T_d) was calculated. This it the average time it takes for a cell population to double in the log-phase and was calculated from the linear part of the curve using following equation [98]:

$$T_d = (t_2 - t_1) \times \frac{ln2}{\ln\left({}^{N_2}/_{N_1}\right)}$$

where N_1 is the confluence (%) at time t_1 and N_2 is the confluecence (%) at time t_2. The estimated population doubling time for HT-29/PAR cells was 29 hours. This is slightly longer than what was found in the literature. Ahmed *et al.* have reported a dobling time at 20-24 hours for HT-29 [99].

3.1.3 Growth curve and population doubling time of HT-29/SR cells

Once the growth curve and population doubling time for HT-29/PAR was established, IncuCyte® experiments with HT-29/SR were performed. This was only performed with 5000 cells per well. HT-29/SR cells were seeded out with 2 μM sunitinib and observed over a period of 140 hours (fig. 22). Based on the calculation with the formula above, the estimated population doubling time for HT-29/SR cells was calculated to 37 hours which is slightly more than observed for HT-29/PAR cells. The cells did not grow confluent (> 80 %) during this time period.

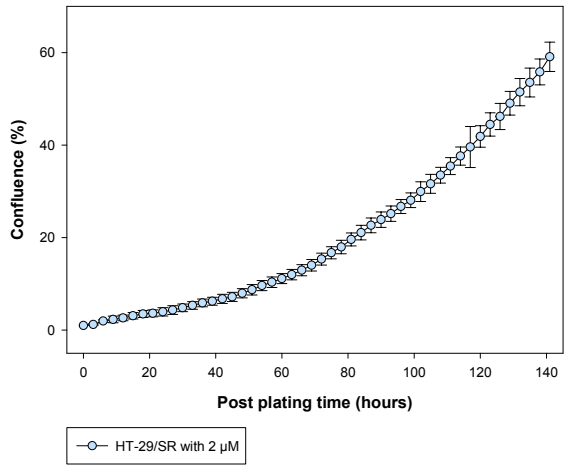

Figure 22 | **Growth curve of HT-29/SR cells with 2 μM sunitinib.** 5000 cells/well were seeded and observed by IncuCyte®. The cells had been treated with sunitinib for 2 months in this experiment. Results from one experiment. Each point is the average of 4 wells.

The doubling time of parental and sunitinib-resistant HT-29 cells have previously been reported by Gotlink *et al.*, where a difference in doubling time was found between the cell lines. It reported a doubling time at ~ 30 hours for parental HT-29 cells, and for sunitinib-resistant HT-29 cells the doubling time was found at ~ 40 hours [9]. Similarly, a difference in doubling time between HT-29/PAR and HT-29/SR cells could be observed here. This is in accordance with the observation in production of the sunitinib-resistant HT-29 cells, where the continuously sunitinib treated HT-29/SR had a lower subcultivation ratio compared to HT-29/PAR cells (section 2.1). The doubling time of HT-29/SR cells was found to be similar in presence of 2 μM sunitinib throughout the thesis.

3.2 Spectral properties of sunitinib

The spectral properties of sunitinib was evaluated by recording absorption and emission spectra. This was important in order to determine if light used for the PCI treatment could interefere with sunitinib and also for fluorescence microscopy. Sunitinib samples were prepared according to procedure 2.6. The maximum absorption of sunitinib was found at 440 nm (fig. 23). Maximum fluorescence was detected at 538 nm (fig. 23). The peaks for absorption and emission of sunitinib are similar to what was found in the literature [95].

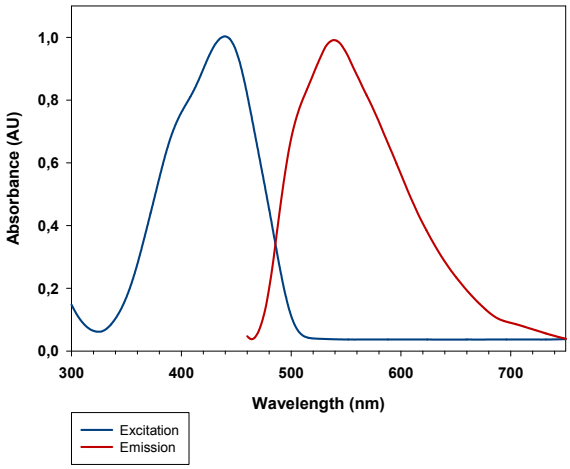

Figure 23 | **Spectral properties of sunitinib.** Normalized absorption and emission spectra of sunitinib (30 μM) in DMSO.

Although the absorbance peak was similar, Nowa-Sliwinska *et al.* reported a somewhat broader absorption range compared to what was found here [95]. This could be due to differences in solvent used. In the present experiment 100% DMSO was used, whereas Nowak-Sliwinska *et*

al. used 0,1% DMSO in 0,9% NaCl solution [95]. An attempt was made here to generate absorption and emission spectra of sunitinib in DMSO and PBS. DMSO was, however, found to be more suitable as PBS gave stuttered signals.

3.3 Sunitinib sensitivity of HT-29/PAR and HT-29/SR cells

The sunitinib sensitivity of HT-29/PAR and HT-29/SR cells were assessed using three different methods; clonogenic assay, MTT assay and IncuCyte®.

3.3.1 Sunitinib sensitivity measured by clonogenic assay

A clonogenic assay was performed according to procedure 2.4.2. This procedure was performed to evaluate the clonogenic capacity of the cell lines in prescence of sunitinib. The clonogeic assay evaluates the long-term effect of sunitinib compared to the MTT assay. The number of cells to seed out in the clonogenic assay was first determined by seeding out different density of HT-29/PAR and HT-29/SR cells. This was performed as different cell lines have different plating efficiencies (PEs). 500 cells per well was found to form sufficiently large colonies within a time period of ≥ 10 days in both cell lines.

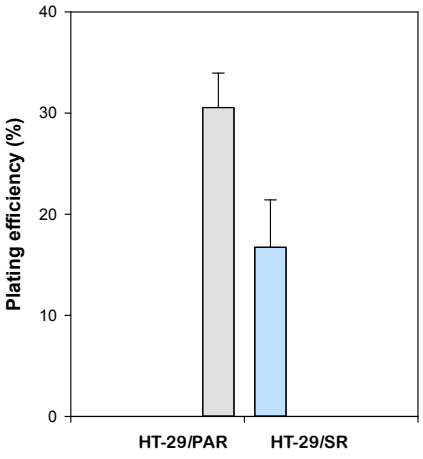

Figure 24 | **Plating efficiency (PE) of HT-29/PAR and HT-29/SR.** PE% = (number of colonies formed)/(number of cells seeded) ×100%. Plating efficiency was calculated based on four clonogenic assays.

HT-29/SR cells were found to have a reduced clonogenic capacity compared to HT-29/PAR cells (p= 0,003) (fig. 24). The difference in PE of HT-29/PAR and HT-29/SR cells was calculated based on the number of colonies in control wells in all clonogenic assays performed

throughout the thesis. HT-29/SR cells was found to have a PE at ~30 %, whereas the PE of HT-29/SR was found at ~17 % (fig. 24). The PE of HT-29/SR was found to be similar throughout the thesis. A reduced PE, in agreement with the present findings has previously been reported by Gotink *et al.* [9]. Another observation that was made in clonogenic assays, was related to the sizes of the colonies. Colonies formed by HT-29/SR were found larger than the parental cells (fig. 25) in the prescence of sunitinib.

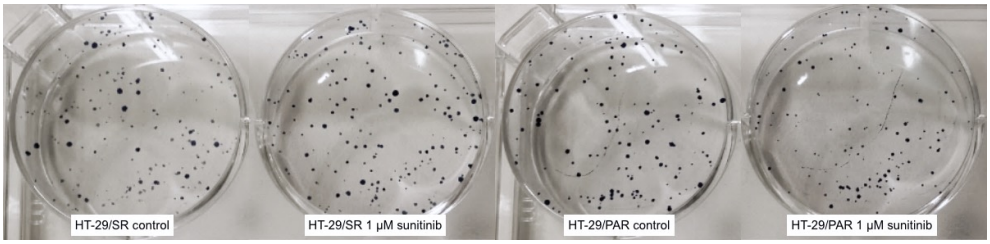

Figure 25 | **Clonogenic assay of HT-29/SR and HT-29/PAR with/without 1 µM sunitinib.** Image of representative wells.

The clonogenic capacity in prescence of sunitinib was evaluated with increasing sunitinib concentration up to 10 µM in both cell lines (fig. 26). However, no large colonies were formed at concentrations higher than 2 µM in neither of the cell lines. In HT-29/SR cells, there were some colonies formed at higher concentrations, but not large enough for counting. The experiment was performed on HT-29/SR cells exposed to sunitinib at 2 and 3,5 months to evaluate if the resistance in HT-29/SR cells changed with time.

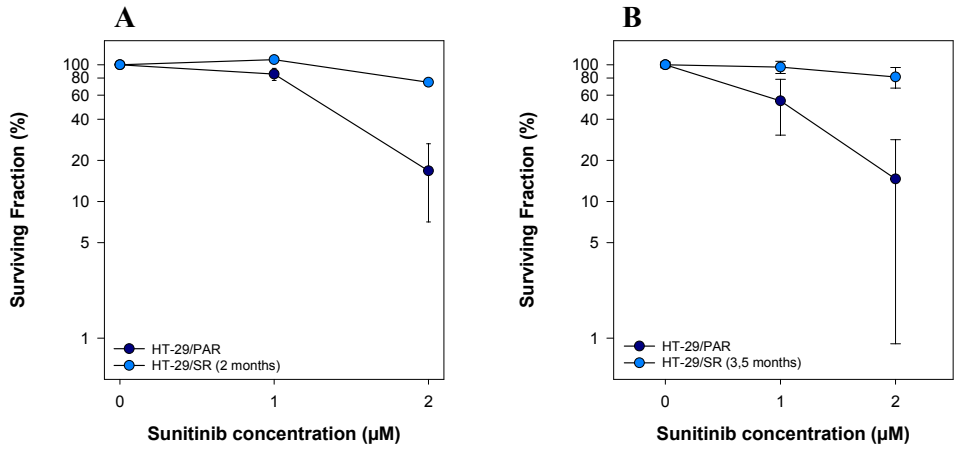

Figure 26 | **Clonogenicity of HT-29/PAR and HT-29/SR cells subjected to increasing sunitinib concentrations for 10 days** (A) HT-29 cells treated with/without sunitinib for 2 months (B) HT-29 cells treated with/without sunitinib for 3,5 months. The graphs are from single experiments. Surviving fraction is relative to an untreated control. Each point is the average of two wells.

Results from fig. 26 indicates that 2 μM does not substantially affect the surviving fraction (SF) of HT-29/SR. After 2 months treatment with sunitinib, 2 μM sunitinib reduced the SF only by 25 % , compared to HT-29/PAR where the SF was reduced by 83 % (fig. 26A). After 3,5 months treatment with sunitinib, the SF after 2 μM sunitinib exposure was reduced by 20 % in HT-29/SR cells, compared with a 76 % reduction in HT-29/PAR (fig. 26B). No large difference in sunitinib sensitivity was detected between HT-29/SR exposed to sunitinib for 2 months and HT-29/SR exposed to sunitinib 3,5 months. However, results from fig. 26 are based on single experiments and these experiments need to be repeated to confirm the effect of sunitinib on clonogenic capacity in HT-29/SR and HT-29/PAR cells. It was attempted several times to repeat these experiments, however, not successful due to problems with dettaching controls during fixation.

3.3.2 Sunitinib sensitivity measured by the MTT assay

The sunitinib sensitivity of HT-29/PAR and HT-29/SR cells was assessed with the MTT assay after 72 hours incubation with sunitinib. The cells were seeded out, and sunitinib was added in different concentrations after attachment. The half maximal inhibitory concentration (IC_{50}) was increased in the sunitinib-resistant cells compared to the parental cells from 2,3 μM to 3,3 μM in the cells treated with sunitinib for 1 month (fig. 27A). This experiment was repeated once with similar results. The MTT assay was also performed at HT-29/SR cells exposed to sunitinib for 3 months. In this experiment IC_{50} for HT-29/PAR was found at 4,8 μM sunitinib and 10 μM for HT-29/SR (fig. 27B). The experiment in fig. 27B was only performed once. Similar experiments were performed during the thesis to obtain sensitivity results on HT-29/SR after sunitinib exposure from 1-5 months. The IC_{50} values obtained were evaluated by calculating a ratio, IC_{50} of resistant cell line/IC_{50} of parental cell line, at each time point which are presented in table 2. The values in table 2 are not reproduced three times. 1 month treatment with sunitinib seemed to induce some resistance. The results may, however, indicate that the resistance increases with time. The experiments must be reproduced twice at each timepoint to conclude.

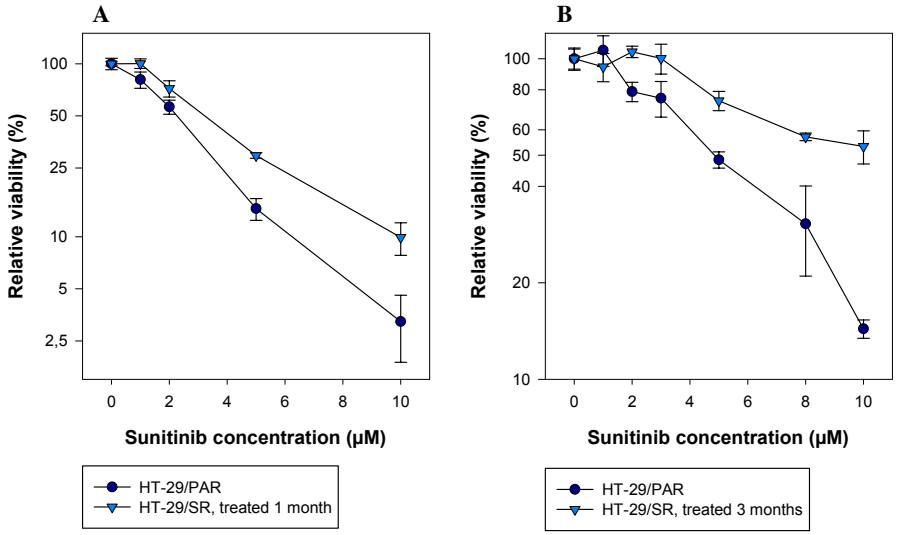

Figure 27 | **72 hours incubation with increasing concentration of sunitinib in HT-29/PAR and HT-29/SR.** (A) HT-29 cells treated with/without sunitinib for 1 month (B) HT-29 cells treated with/without sunitinib for 3 months. The graphs are from single experiments. Viability (MTT) is relative to untreated cells on the same plate. Each point is the average of 3 wells.

	HT-29/SR IC_{50} (µM)	**HT-29/PAR IC_{50} (µM)**	**Ratio**
1 month	3,3	2,3	1,43
3 months	10	4,8	2,08
3,5 months	6,0	4,1	1,46
4 months*	7,5	4,5	1,67
5 months	8,2	4,1	2,00
5 months**	6,5	4	1,63

Table 2 | **IC_{50} values of sunitinib in HT-29/PAR and HT-29/SR cells with increasing time to obtain resistance.** MTT assay performed 72 hours after sunitinib incubation. A ratio was calculated by dividing IC_{50} for HT-29/SR cells with IC_{50} for HT-29/PAR cells. *48-hour incubation **96-hour incubation

3.3.3 Sunitinib sensitivity measured by growth curves

HT-29/PAR and HT-29/SR cells were observed in IncuCyte® in the presence of sunitinib at different concentrations, ranging from 0 to 10 μM, and observed over a period of 140 hours. The procedure for IncuCyte® is described in section 2.4.3.

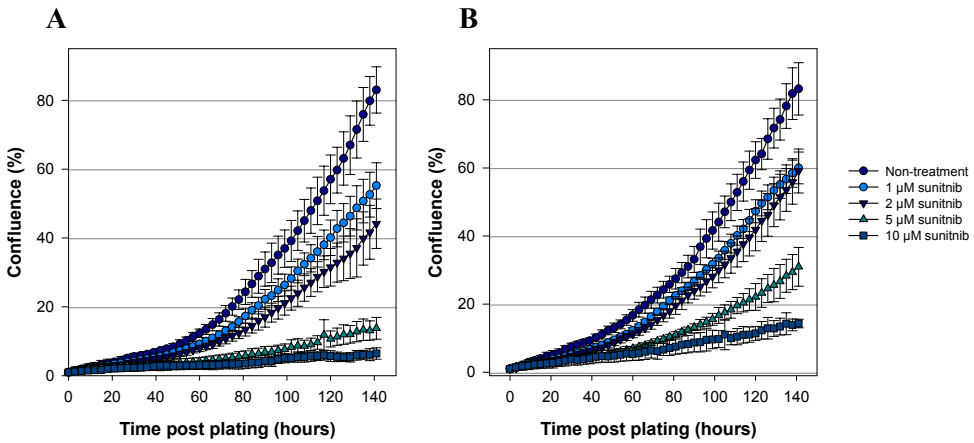

Figure 28 | **Growth of HT-29/PAR and HT-29/SR cells at increasing sunitinib concentrations over 140 hours.** (A) HT-29/PAR cells and (B) HT-29/SR cells (3 months sunitinib-treatment). The graphs are from a single experiment. Confluence (%) is relative to non-treated cells. Each point is the average of four wells.

The HT-29/PAR cells that were plated without sunitinib reached 50 % confluence after 111 hours compared to 108 hours for HT-29/SR cells. At 1 μM sunitinib, HT-29/PAR cells reached 50 % confluence after 132 hours and HT-29/SR cells after 123 hours. At sunitinib concentrations higher than 1 μM sunitinib, HT-29/PAR cells did not reach 50 % confluence and at 10 μM sunitinib the HT-29/PAR cells did not even reach 10 % confluence. Based on these results, HT-29/SR cells are capable to proliferate at higher sunitinib concentration compared to the parental cells. The data from figure 28 are presented in table 3. The effect of sunitinib on growth is evident at all concentrations indicating that the growth of the cells are slower in prescence of sunitinib and sunitinib-resistance is induced in HT-29/SR cells. The results here are, however, from one experiment, and should be performed at different timepoint in order to evalute the effect of sunitinib on growth in HT-29/SR cells over time.

Sunitinib concentration Confluence	**Control** 50 %	**1 μM** 50 %	**2 μM** 20 %	**5 μM** 20 %	**10 μM** 10 %
HT-29/PAR	111	132	96	117	N/A
HT-29/SR	108	123	81	75	105

Table 3 | **The effect of sunitinib on HT-29/PAR and HT-29/SR cells measured by hours to reach a certain percentage of confluence.** Calculated based on the average of four wells. HT-29/SR cells had been treated with sunitinib for 3 months.

3.4 Uptake and cellular localization of sunitinib in HT-29/PAR and HT-29/SR cells

3.4.1 Fluorescence microscopy of sunitinib

The intracellular localization of sunitinib was detected with fluorescence microscopy in order to confirm the localization in acidic organelles. The samples were prepared according to procedure 2.5.1 for both HT-29/PAR and HT-29/SR cells. Sunitinib (green) and LysoTracker Red® (red) were found to be highly co-localized (yellow) in both cell lines (fig. 29). Gotink *et al.* has previously reported that sunitinib localize in acidic vescicles, and also a higher sequestration of sunitinib in sunitinib-resistant cells compared to parental cells [9].

It was attempted to acquire fluorescence images with the same exposure time for HT-29/SR as for HT-29/PAR, for comparison. However, this was problematic as the cellular uptake of sunitinib varied within the cell lines. In some cases, image acquisition of HT-29/PAR cells with same exposure time as HT-29/SR cells gave overexposure indicating more sunitinib present in the parental cell line compared to the sunitinib-resistant cell line. Fluorescence microscopy with lower magnification, 20x, was also attempted in order to acquire images of more cells at the same time. With lower magnification, fluorescence from sunitinib and the other fluorescence agents could not be detected.

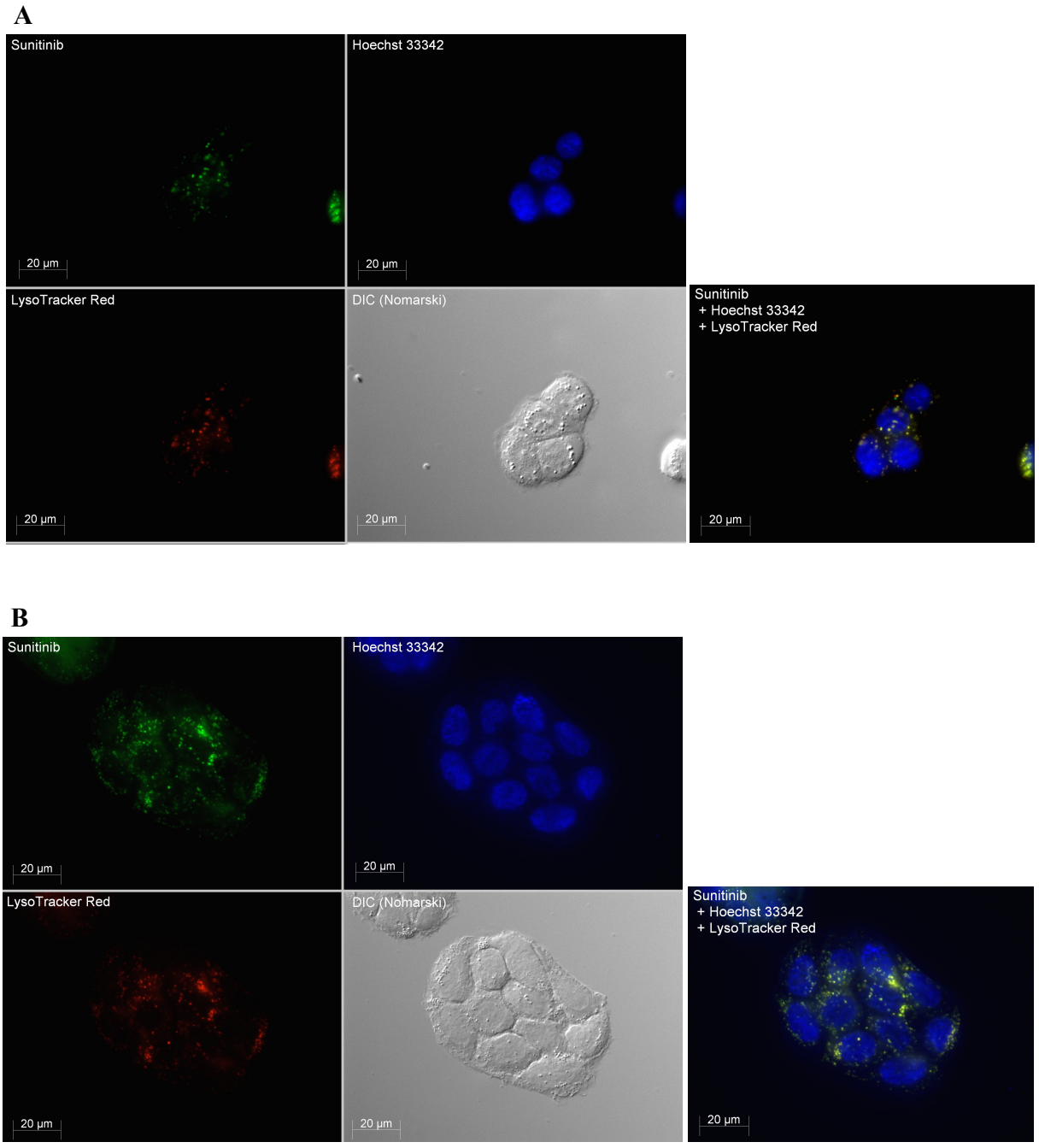

Figure 29 | **Cellular localization of sunitinib.** (A) HT-29/PAR (sunitinib exposure time 118 ms) (B) HT-29/SR (sunitinib exposure time 105 ms). Fluorescence and phase contrast microscopy performed on HT-29/PAR and HT-29/SR following a 24 hour-incubation with 2 µM sunitinib (green). The nucleus was stained with Hoechst 33342 (blue) and lysosomes with LysoTracker Red® (red). Images acquired with 63x magnification. Scale bars are 20 µm. Representative images from one experiment.

Although a difference in fluorescence could not be detected between the cell lines, it was observed during the thesis a difference in the cell pellet color of HT-29/PAR cells compared to HT-29/SR cells. Sunitinib stock solution had a bright yellow color, and a faint yellow could be

observed in HT-29/SR cell pellets whereas the HT-29/PAR cell pellets were more towards pink, which may indicate accumulated sunitinib in HT-29/SR cells over time.

3.4.2 Flow cytometry analysis: uptake of sunitinib

Relative quantification of fluorescence images can be difficult as the fluorescence measurements can be affected by the samples, the microscope or/and the detector. The sunitinib uptake was therefore quantified with flow cytometry analysis. The samples were prepared according to procedure described in 2.5.3. The cells were first kept 48 hours in sunitinib-free medium followed by 24 hours incubation of sunitinib. Flow cytometry results revealed a large shift in the fluorescence intensity in cells that were subjected to sunitinib, but there were no difference between cellular uptake in HT-29/PAR and HT-29/SR cells (fig. 30). The cells lines were compared by subtracting the fluorescence intensity of non-treated cells from treated cells, and calculating the ratio between HT-29/PAR and HT-29/SR. The ratio of fluorescence intensity between the cell lines was found to be ≈ 1.

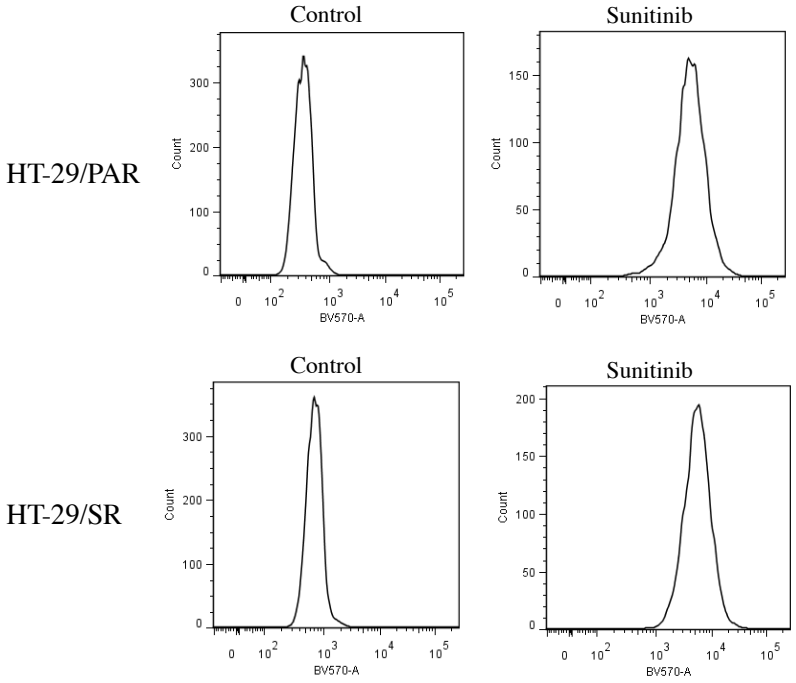

Figure 30 | **Cellular uptake of sunitinib.** BV570-A = fluorescence intensity. Representative flow cytometry charts from one experiment.

3.5 Cellular localization of $TPCS_{2a}$

Drug delivery with PCI is dependent on the PS's localization on the membrane of the endocytic vesicles. $TPCS_{2a}$ is amphiphilic and is expected to be localized in endocytic vesicles after being subjected to adsorptive endcytosis (section 1.5.1). The cellular localizaion of $TPCS_{2a}$ in HT-29/PAR was detected with fluorescence microscopy following 18 hour-incubation. This was performed both with and without 2 hours chase in HT-29/PAR cells. The samples were prepared according to procedure in 2.5.1. In the cells without chase, a diffuse fluorescence could be observed. The diffuse fluorescence was probably due to the plasma membrane bound $TPCS_{2a}$. Cells that were chased for 2 hours did not have the same diffuse fluorecence. Some co-localization (yellow) of $TPCS_{2a}$ (red) and Lysotracker Green® (green) could be observed in both HT-29/PAR cells with and without 2 hour chase, indicating prescence of $TPCS_{2a}$ in endocytic vesicles (fig. 31).

Evaluation of the cellular localization of $TPCS_{2a}$ in HT-29/SR was not performed, but should be included in future experiments to confirm that the $TPCS_{2a}$ is localized in the endocytic vesicles also in these cells. It might also be wise to evaluate the cellular localization in both cell lines after 4 hours chase, which is the chase time used for PCI experiments.

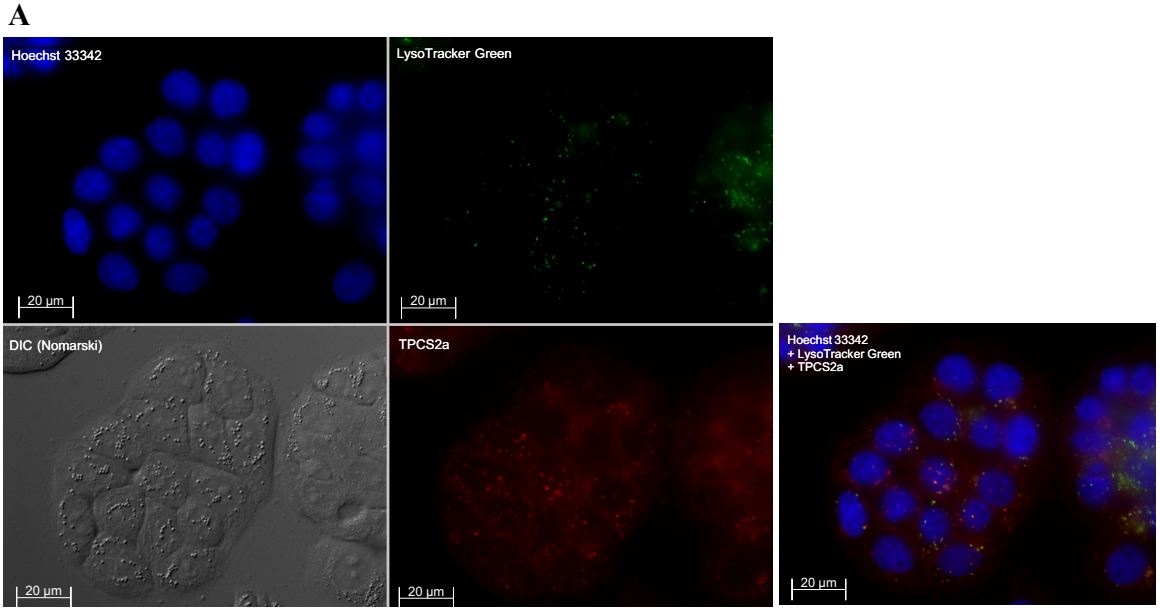

B

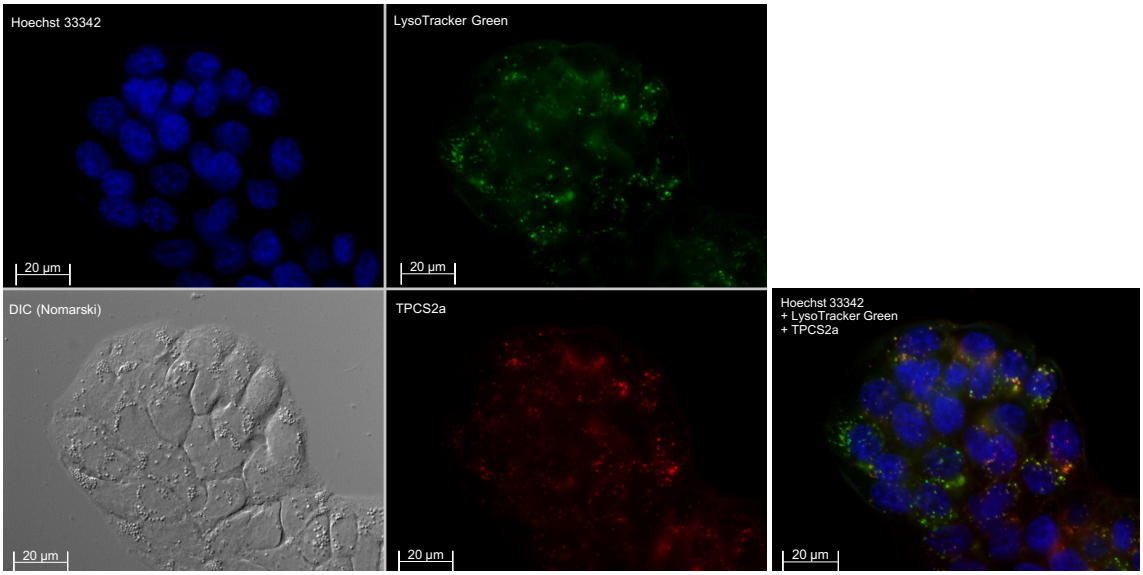

Figure 31 | **Co-localization of $TPcS_{2a}$ and LysoTracker Green® in HT-29/PAR cells.** Fluorescence and phase contrast microscopy performed on parental HT-29 after incubation of 0,4 µg/ml $TPcS_{2a}$ for 18 hours (A) and including 2 hour-chase (B) in drug-free medium The nucleus was stained with Hoechst 33342 (blue) and lysosomes with LysoTracker Green® (green). Scale bars are 20 µm. Images were acquired with 63x magnification. Representative images from one experiment.

3.6 PCI of sunitinib in HT-29/PAR and HT-29/SR cells

Since lysosomal sequestration of sunitinib was indicated as a potential resistance mechanism [9], it was hypothesized that PCI could overcome the resistance. Preliminary experiments by Dr. Anette Weyergang, using the "light after" PCI procedure of sunitinib in HT-29/PAR and HT-29/SR cells with blue light showed antagonistic effects between sunitinib and PDT. The spectral properties of sunitinib was proposed to be a cause of this antagonism. Since sunitinib absorbs light in the blue region, red light was used here in PCI experiments with sunitinib.

3.6.1 PDT red light with $TPCS_{2a}$

To establish the optimal light dose for PCI treatment with red light, the phototoxicity of 0,4 µg/ml $TPCS_{2a}$ was investigated at different light doses. PDT curves were established for both HT-29/PAR and HT-29/SR cells. The cells were treated accordig to the standard PDT procedure (section 2.3.2) and treated with light does ranging from 0 to 350 seconds (0-2.1 J/cm^2). The

MTT assay (section 2.4.1) was used to evaluate the viability 48 hours post-illumination (fig. 32).

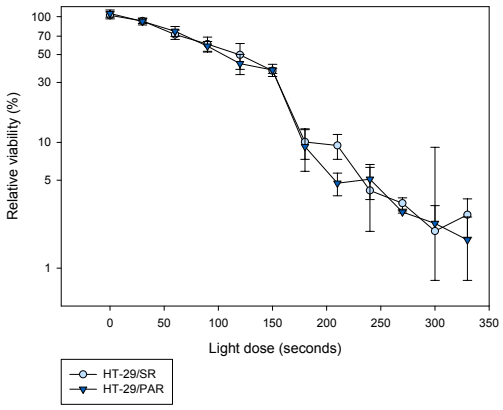

Figure 32 | **PDT curves for HT-29/SR and HT-29/PAR cells subjected to red light (650-660 nm).** HT-29/SR cells were treated with sunitinib for 2 months. Representative result from one experiment. Cells viability (MTT) is presented relative to untreated cells on the same plate. Each point is the average of three wells.

Both cell lines responded similarly to the PDT treatment (fig. 32), and based on all experiments, 90 seconds was chosen for subsequent PCI experiments. This light dose reduced the viability by about 30 %, which previously has been reported to be sufficient for drug delivery by PCI [1].

3.6.2 PCI of sunitinib "light after"-procedure

The standard procedure of PCI is the "light after"-procedure, and this was the first procedure explored with HT-29/PAR and HT-29/SR cell lines. To establish an optimal "light after"-procedure, different parameters were investigated including co-incubation of sunitinib and $TPCS_{2a}$, increasing incubation time of sunitinib and increasing incubation time from illumination to the MTT assay. Both light dose- and sunitinib concentration-dependent PCI experiments were performed in HT-29/PAR and HT-29/SR cells. The result are shown in figure 33-35.

One of the first PCI experiments of sunitinib was performed with increasing light doses (red light), ranging from 0 to 350 seconds, and fixed sunitinib dose, 2 μM sunitinib, which was co-incubated with $TPCS_{2a}$ (fig. 33). 18 hour-incubation of sunitinib was thought to be sufficient for lysosomal accumulation. Lysosomal accumulation of sunitinib has previously been detected in HT-29 cells by fluorescence microscopy after only 1 hour incubation [9]. The same sunitinib dose for HT-29/PAR and HT-29/SR was used. The MTT-assay was performed 48 hours after

illumination. No difference between PDT and PCI treatment could be observed in the HT-29/PAR and HT/SR cell lines. However, the effect of sunitinib (2 μM) for 18 hours did not significantly influence on the viability, and the concentration and/or incubation time could been increased to evaluate if this would have caused an effect of PCI.

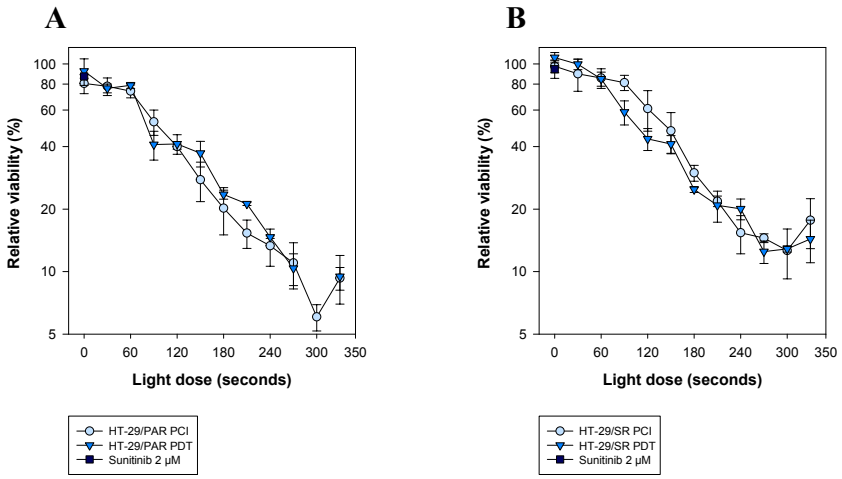

Figure 33 | **PCI "light after"-procedure with increasing light doses of 2 μM sunitinib.** (A) HT-29/PAR cells and (B) HT-29/SR cells. The figures show representative results from a single experiment. Cell viability (MTT) is relative to untreated cells on the same plate. Each point is the average three wells.

The procedure was therefore changed to 48 hours sunitinib incubation and 72 hours from illumination to MTT-assay (results not shown). Similar results as shown in fig. 33 was, however, observed. HT-29/SR cells had at this point been treated with sunitinib for 2,5-3 months.

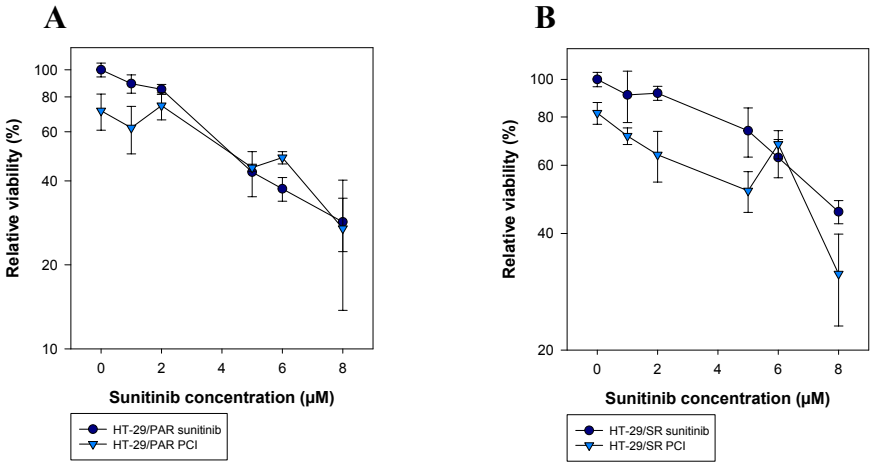

Figure 34 | **PCI "light after"-procedure with increasing concentration of sunitinib.** (A) HT-29/PAR cells ans (B) HT-29/SR cells. The cells were subjected to PCI of sunitinib using the "light after"-procedure 48 hours of incubation with sunitinib and 72 hours of incubation post illumination with 90 seconds of red light. Representative

results from a single experiment. Cells viability (MTT) is relative to untreated cells on the same plate. Each point is the average of three wells.

PCI experiments were also performed with increasing sunitinib concentrations, up to 8 μM, with fixed light dose (90 seconds) (fig. 34). In these experiments the curves for sunitinib and PCI intersect, indicating an antagonistic effect (fig. 34). In HT-29/SR cells, the intersection is at higher concentrations (6-8 μM). HT-29/SR had at this point been treated with sunitinib for 3-4 months.

To further confirm the antagonistic effect, clonogenic assays were performed to assess the effect of "light after"-procedure with red light (fig. 35). This was performed according to the standard PDT/PCI procedures where the cells were incubated with 1 μM sunitinib 48 hours prior to illumination. 6-well plates requires higher light dose than 96-well plates. The 6-well plates were subjected to light doses of 110 and 130 seconds (fig. 35). The colonies were fixated and colored (section 2.4.2) 10 days after illumination when visible colonies were formed in the controls. No difference between PCI and PDT could be observed (fig. 35). However, this experiment was only performed. The sunitinib and light doses used in this experiment may not have been optimal. HT-29/SR had at this point been treated with sunitinib for 4 months.

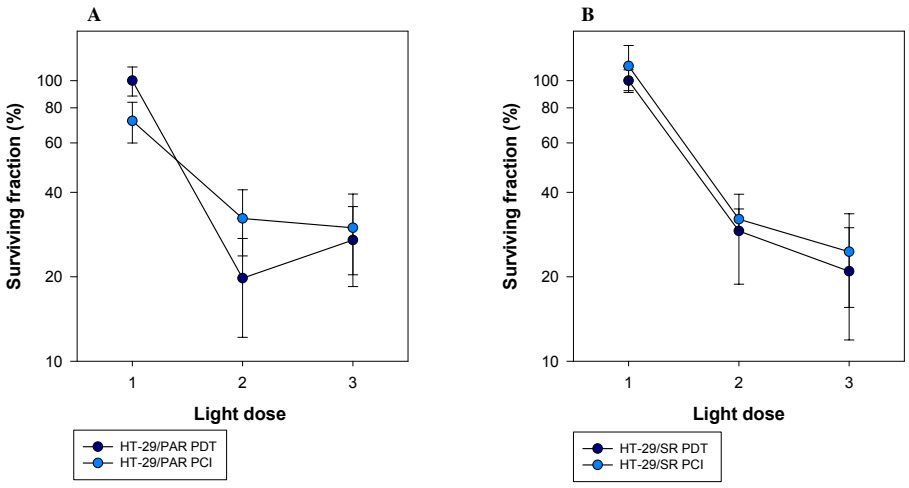

Figure 35 | **Clonogenic survival after PDT and PCI of 1 μM sunitinib.** (A) HT-29/PAR and (B) HT-29/SR. Cells viability is relative to an untreated control on the same plate. Results from one experiment. Each point is the average of three wells. Light dose 1= 0 seconds, 2 = 110 seconds, 3= 130 seconds.

3.7 Co-localization of sunitinib and $TPCS_{2a}$ in HT-29/SR cells

3.7.1 Co-localization of $TPCS_{2a}$ and sunitinib

It was hypothethized that both sunitinib and $TPCS_{2a}$ were localized in the membrane of endocytic vesicles. This may explain why the "light after" procedure was not successful in this cell line. If sunitinib is localized close to $TPCS_{2a}$, it could potentially be destroyed by ROS generated during the photochemical reaction. Super-resolution microscopy was employed in order to visualize the localization of $TPCS_{2a}$ and sunitinib in HT-29/SR cells (fig. 36 and 37). The cells were prepared according to procedure 2.5.2, and the results indicated both $TPCS_{2a}$ and sunitinib to be present in membranes of the endocytic vesicles in HT-29/SR cells.

Images in figure 36 and 37 are acquired with SIM (structured illumination microscopy) approach which is a technique used to improve resolution by reconstruction from a set of images taken. In figure 36, the images are reconstructed based on seven optical sections. White arrows on the figure indicate co-localization of sunitinib and $TPCS_{2a}$ in ring-like structures, resembling endocytic vesicles. The ring-like structures with empty lumen were visualized more clearly in magnified images (fig. 37). One pixel in the image is equivalent to 40 nm, and the diameter of this ring-like structure is approximately 500 nm (fig. 37B), in accordance with size of endocytic vesicles [100].

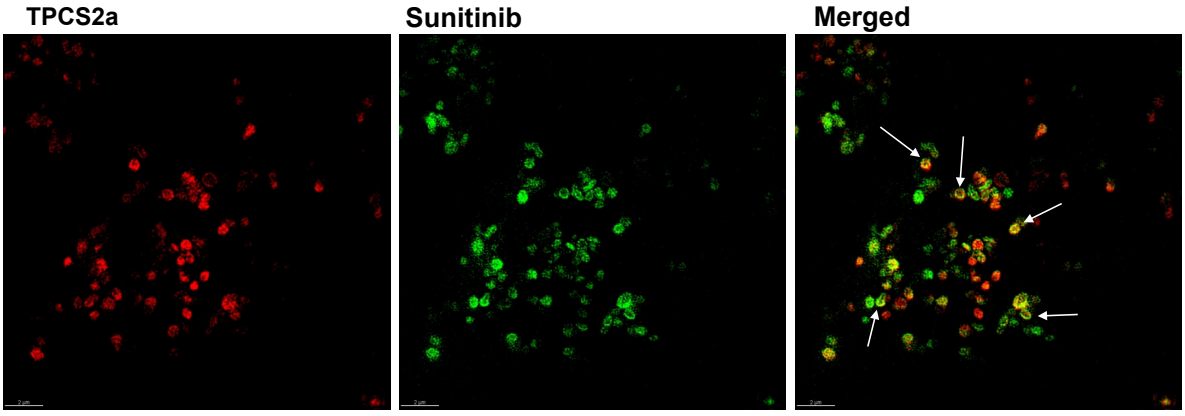

Figure 36 | **Super-resolution microscopy of sunitinib (green) and $TPCS_{2a}$ (red)**. White arrows indicate co-localization (yellow). Representative images from one experiment. Scale bars are 2 μm.

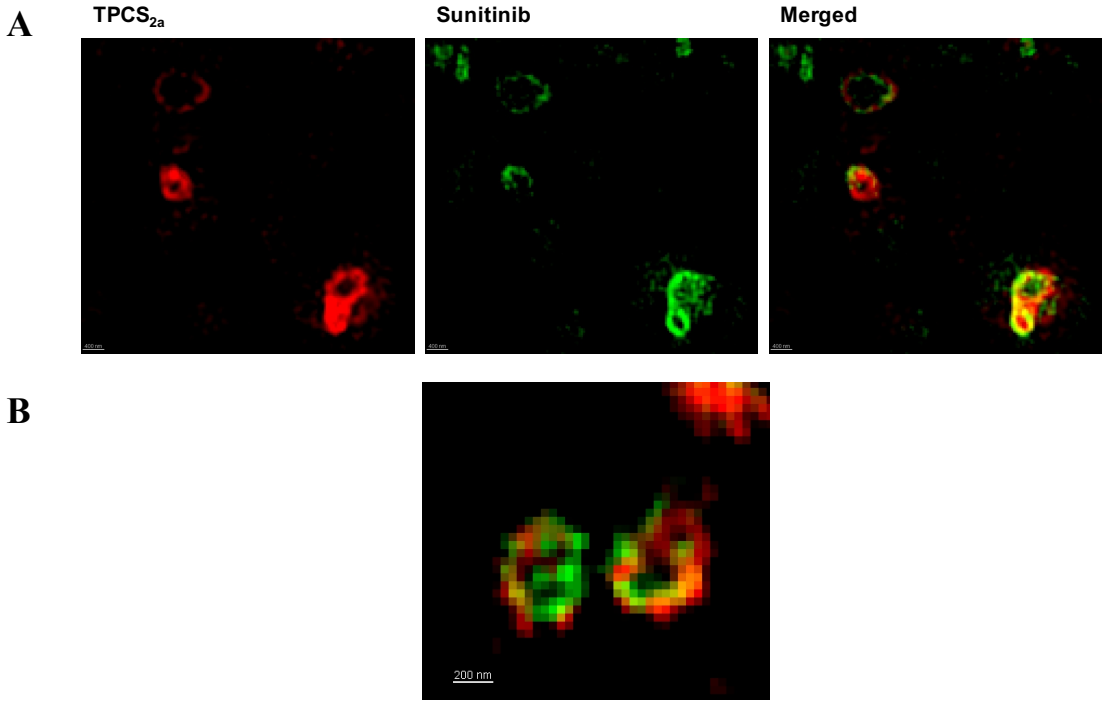

Figure 37 | **Magnified images of co-localization of sunitinib and $TPCS_{2a}$.** Ring-like structures with co-localization (yellow) of sunitinib (green) and $TPCS_{2a}$ (red). (A) Reconstruction of three images. Scale bar = 400 nm (B) Reconstruction of two images. One pixel is equivalent to 40 nm. Scale bar = 200 nm.

3.8 PCI of sunitinib with "light first"-procedure

"Light first"-procedure was performed since it was hypothesized that $TPCS_{2a}$ also in combination with red light reduced the toxic effect of sunitinib, and destruction of sunitinib was the cause of the apparent antagonistic effect (fig. 33-35). The PCI experiments was therefore performed with the cells treated according to the procedure in section 2.3.2, and the MTT assay was performed 72 hours post-illumination. The cells were subjected to 90 seconds red light. The results indicated the "light first" procedure as a potential strategy for intracellular drug delivery of sunitinib.

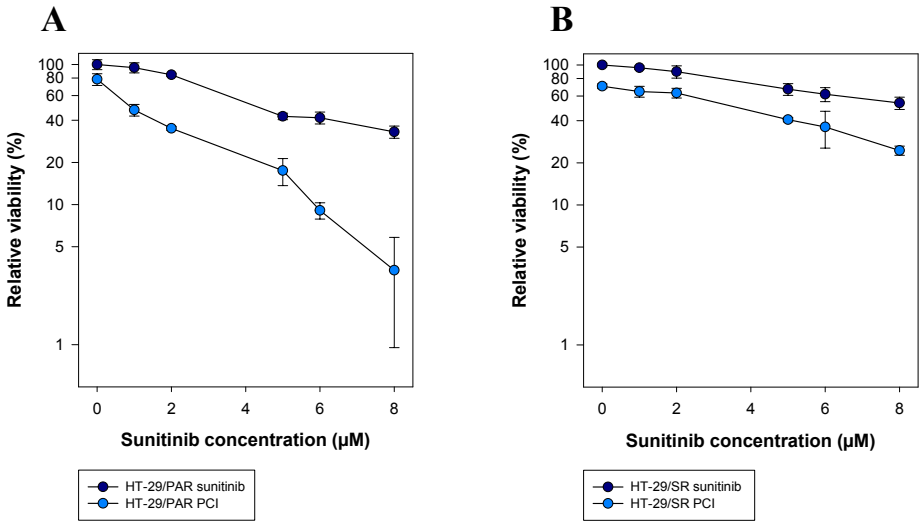

Figure 38 | **PCI "light first"-procedure with increasing concentration of sunitinib.** (A) HT-29/PAR cells and (B) HT-29/SR cells were treated with PDT (red light) for 90 seconds followed by 72 hour-incubation of sunitinib. Cells viability (MTT) is relative to untreated cells on the same plate. Results from one single experiment. Each point is the average of three wells.

PDT alone induced a 20 % reduction in viability, and 1 μM sunitinib alone reduced the viability by 5 % in HT-29/PAR cells (fig. 38A). PCI of 1 μM sunitinib in this cell line induced 53 % reduction in viability which is more than PDT and sunitinib effect combined (fig 38A). In HT-29/SR cells the PDT dose in this experiment induced a 29 % reduction in viability, and 8 μM sunitinib reduced the viability by 46 %. PCI in these cells at 8 μM induced 75 % reduction in viability, however this seems not more than the PDT and sunitinib effect combined (fig. 38B). The HT-29/SR cells had at this point been treated with sunitinib for 4,5-5 months. The results therefore indicate PCI with "light first"-procedure as a better strategy for delivery of sunitinib to the HT-29/PAR cells, and a PCI effect might have been observed at higher concentrations for HT-29/SR cells. This experiment is only performed once, and needs to be reproduced twice in order to confirm.

3.9 PCI of recombinant toxin gelonin (rGel) in HT-29/PAR and HT-29/SR cells

Type I RIPs are good candidates for PCI as described in section 1.5.2. The PCI effect of rGel in HT-29/PAR and HT-29/SR cell lines was evaluated. These experiments were performed to evaluate if PCI is a feasible drug delivery method in both of these cells lines. Most of the

experiments with rGel in this thesis has been on HT-29/PAR cells with blue light, and were performed during the period when the resistant of HT-29/SR cell line was made.

3.9.1 Cytotoxicity of rGel in HT-29/PAR cells

Initially, 50 nM rGel was used in the first PCI experiment. The cells were incubated with rGel 4 hours prior to illumination. This procedure did not reveal any reduction in viability alone nor by PCI (results not shown). The incubation time was therefore increased, and the toxicity of rGel in HT-29/PAR was evaluated by incubating the cells with increasing rGel concentrations for 18 hours to find the optimal concentration for PCI experiments. Ideally, the concentration of rGel should reduce the viability by 10-30 % alone in PCI experiments [1]. The cells were incubated with rGel for 18 hours before wash and 4 hours chase in drug-free medium. HT-29/PAR cells was subjected to rGel in concentrations ranging from 0,01 μM up to 10 μM (fig. 39). The MTT assay was performed 48 hour after. Reduction in viability could be observed at concentrations above 0,5 μM. At 0,5 μM rGel, it induced about 20 % reduction in viability.

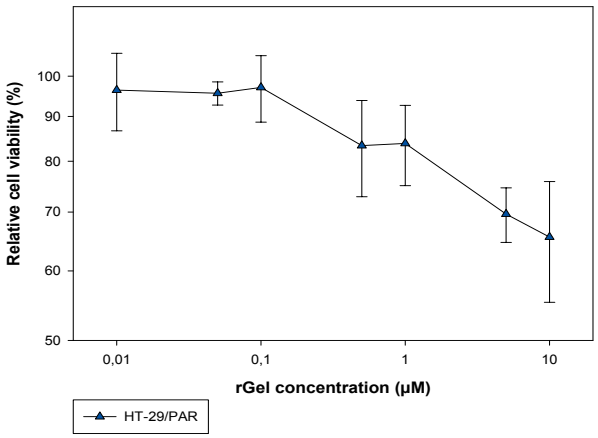

Figure 39 | **Relative viability of rGel in HT-29/PAR cells.** Representative results from one experiment. Cells viability (MTT) is relative to untreated cells on the same plate. Each point is the of three wells.

3.9.2 PDT blue light with $TPCS_{2a}$ in HT-29/PAR cells

The PDT effect with blue light were explored on HT-29/PAR cells with 0,4 μg/ml $TPCS_{2a}$ and increasing light doses, ranging from 0 to 120 seconds (0-1,4 J/cm^2). The MTT assay was performed 48 hours after illumination.

Shorter illumination time is required using blue light compared to red light (fig. 32). The blue region of the absorption spectra has shorter wavelengths thus higher energy (section 1.4.4). LumiSource™ also has a broader emission peak and fluence rate (section 2.3.1) compared to the red light used in this thesis. The cells were treated according to the standard PDT procedure (section 2.3.2). At a light dose of 60 seconds, the relative cell viability had been reduced by about 40 %. This was the light dose chosen for PDT/PCI experiments with blue light.

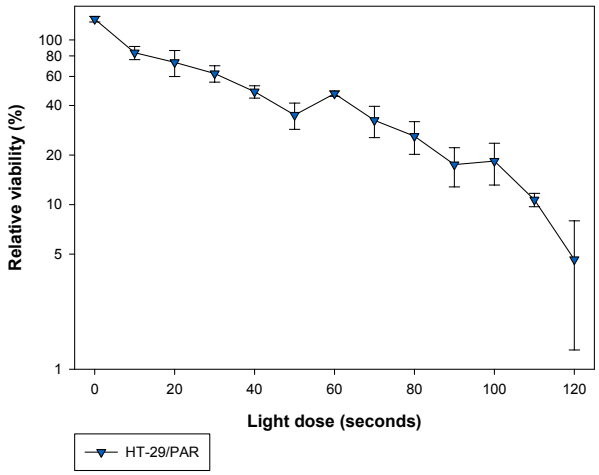

Figure 40 | **PDT curve for HT-29/PAR cells subjected to $TPCS_{2a}$ and blue light (~ 435 nm).** The figure shows a representative result from a single experiment. Cells viability (MTT) is relative to untreated cells on the same plate. Each point is the average of three wells.

3.9.3 PCI of rGel in HT-29/PAR and HT-29/SR cells

PCI experiments with rGel were performed with the "light after"-procedure. The cells were treated according to the standard PDT/PCI procedures (section 2.3.2.) and blue light.

rGel concentration dependent PCI experiments

The "light after"-procedure with increasing rGel concentration was performed in both cell lines. The MTT assay was performed 48 hours after illumination. The HT-29/SR cells' reponse to rGel and blue light had not been tested prior to these experiments. These results (fig. 41) showed, however, a similar response to rGel in the cell lines. A similar response in the cell lines was also found following PCI using 60 seconds of blue light (fig. 41).

The results indicate that rGel alone in this concentration range induced only a slight reduction in viability (fig. 41). At 0,1 μM, rGel alone or with PCI did not affect the viability in neither of

the cell lines. At 0,5 µM, the relative cell viability is reduced by 20 % in HT-29/PAR and 15 % in HT-29/SR which are in accordane to the results found in section 3.9.1 (fig. 39). PDT alone induced a 39 % and 44 % reduction in viability in HT-29/PAR and HT-29/SR, respectively (not shown in fig. 41). PCI of 0,5 µM rGel reduced the viability of HT-29/PAR cells by 68 % and in HT-29/SR cells, the viability was reduced by 74 % (fig 41). This is more than PDT alone and rGel alone combined. These results indicate that PCI is a feasible drug delivery system of rGel in both cell lines.

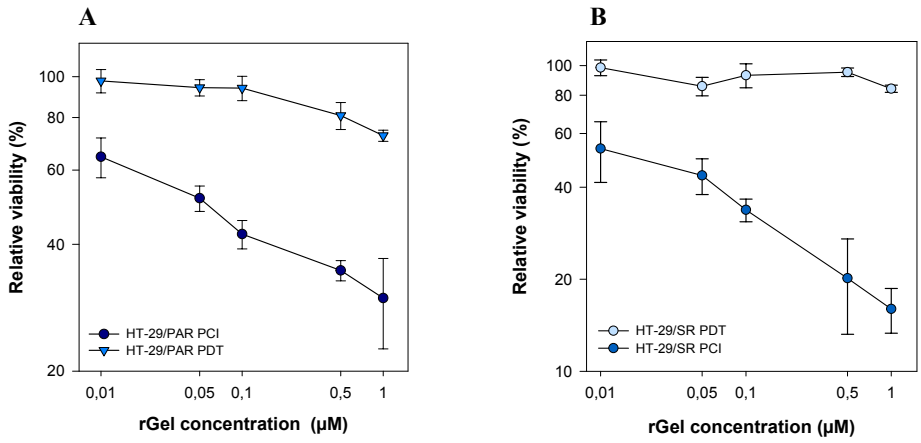

Figure 41 | | **PCI "light after"-procedure with increasing concentration of rGel** (A) HT-29/PAR cells (B) HT-29/SR cells treated with sunitinib for 4 months. Representative results from one experiment. The cells were subjected to 60 seconds blue light. Cells viability (MTT) is relative to untreated cells on the same plate. Each point is the average of three wells.

4 Discussion

RTKs are involved in a number of cellular signalling pathways and regulate several critical processes that are important for tumor progression, including tumor angiogenesis which has been linked to metastasis [20]. RTKs comprise of an extracellular domain for ligand-binding and an intracellular domain with kinase activity that initiates a number of signalling cascades linked to survival and proliferation [3]. A number of cancer therapeutics have therefore been specifically developed to interfere with RTK signalling, these therapeutics includes TKIs [36]. TKIs are small molecules that are capable to penetrate the plasma membrane and bind to the intracellular domain of RTKs where they can inhibit signalling [3, 32]. However, development of drug resistance against TKIs during treatment is an important clinical problem [3, 32, 34]. A number of resistance mechanisms have been linked to TKIs, and also for sunitinib, where lysosomal sequestration been proposed amongst other [3, 9].

Theoretically, there are two approaches that can be employed to overcome drug resistance in cancer; the first is a mechanistic approach toward the cause of the resistance [1]. A mechanistic approach targets the mechanism of drug resistance, for instance inhibition of P-gp by verapamil [1]. However, this strategy is associated with tolerability problems due to low selectivity of such inhibitors [1, 75]. The second strategy to overcome drug resistance is resistance circumvention where the resistant cells are subjected to a treatment not captured by the mechanism of resistance [1]. PCI has been proposed as a strategy for resistance circumvention [1]. This is a strategy that takes advantage of therapeutics trapped in endocytic vesicles and uses non-lethal light to induce destabilisation of endo/lysosomal membrane, and thereby release of the entrapped drug [1]. However, PCI should also be able to act as an mechanistic approach when the mechanism is lysosomal sequestration. PCI has been shown to reverse doxorubicin resistance in breast cancer cells, where doxorubicin was lysosomal sequestrered [82]. PCI as a strategy to bypass resistance has been found feasible in a number of cell lines *in vitro* as well as *in vivo* [1, 76]. In this thesis, PCI was investigated as a drug delivery system for sunitinib in both parental and sunitinib-resistant HT-29 cells.

A number of publications related to PCI are described for macromolecules [76]. However, PCI has also been shown to be feasible for small-molecular therapeutics [76]. Currently, a phase I/II Amphinex®-based PCI study with the small molecule cytostatic gemcitabine is enrolling patients (ClinicalTrials.gov identifier: NCT01900158). Previously, a synergistic effect has been

reported by $TPPS_{2a}$-PDT targeted to the endocytic vesicles followed by administration of tyrphostin AG1478 [101]. Tyrphostin is a EGFR specific TKI with structural similarities to clinical used gefitinib and erlotinib [101]. Although this was not termed PCI, the procedure used in this publication is similar to the one used here ("light first"-procedure) [101].

Acquired sunitinib-resistant HT-29 cells have previously been studied by Gotink *et al.*, and some similarities could be found when compared to the HT-29/SR cells established here [9]. Gotink *et al.* established their resistant HT-29 cells by continuous exposure of sunitinib for more than 12 months, and gradually increased the concentrations of sunitinib up to 12 μM, a concentration which killed the parental cells [9]. Whereas the procedure used here included continuous sunitinib exposure at 2 μM over a period of 1-5 months. The sunitinib concentration used here induced only ~ 20 % reduction in viability in parental HT-29 cells. The sunitinib sensitivity was in this present thesis studied in HT-29/PAR and HT-29/SR cells, and the results showed a dose-dependent effect of sunitinib in both cell lines in agreement with previous publications [9, 30]. We here obtained the lowest IC_{50} value for HT-29/PAR at 2,3 μM and a low IC_{50} at 3,3 μM, which was observed in HT-29/SR after only 1 month of sunitinib exposure (table 2). Gotink *et al.* reported that the IC_{50} value increased in the sunitinib-resistant HT-29 cells from 1,9 μM to 3,5 μM [9]. The IC_{50} values found throughout this thesis varied slightly, however, the ratios measured by IC_{50} (HT-29/SR)/ IC_{50} (HT-29/PAR) were in the same range, as published by Gotink *et al.*, (1,45-2,08 by us, and 1,7 by Gotink *et al.*) [9]. The sunitinib-sensitivity HT-29/PAR and HT-29/SR cells was further documented by experiments on clonogenic capacity and effect on population doubling time. It is not clear to us how Gotink *et al*. would obtain such a low IC_{50} value for sunitinib in the resistant cell line after continuous exposure of sunitinib in concentrations up to 12 μM.

An observation made during this thesis, was the cell pellet color of HT-29/PAR compared to HT-29/SR cells. The sunitinib stock solution had a bright yellow color, and a faint yellow could be observed in HT-29/SR cell pellets whereas the HT-29/PAR cell pellets were toward a pink tone. This observation supports the assumption that sunitinib is accumulated in HT-29/SR cells over time, although experiments need to be perfomed to confirm. A higher lysosomal sequestration of sunitinib has previously been reported in resistant HT-29 cells compared to parental HT-29 cells [9]. Gotink *et al.* evaluated this by fluorescence microscopy, and further supported the finding with Western blot analysis that revealed increased expression of major lysosome-associated membrane protein (LAMP)-1 and LAMP-2 in sunitinib-resistant HT-29

cells compared to their parental cell [9]. The intracellular localization of sunitinib was also investigated in this thesis by fluorescence microscopy. Sunitinib was found to localize in acidic subcellular compartments with LysoTracker staining, also in our resistant model. However, no difference in localization could be observed between HT29/PAR and HT-29/SR cells. It was difficult to compare the two cell lines due to variations in sunitinib fluorescence within the cell line. Although further fluorescence experiments are needed to confirm lysosomal sequestration as a resistance mechanism in the HT-29/SR cells, endocytic localization of sunitinib was confirmed in both parental and resistant HT-29 cells, thus PCI experiments were performed on both cell lines.

To further evaluate the intracellular concentration of sunitinib in HT-29/PAR and HT-29/SR cells, flow cytometry was employed. No difference in the fluorescence intensity was, however, observed between the cells lines. Gotink *et al.* found a difference in intracellular sunitinib concentration in their sunitinib-resistant HT-29 cells compared to the parental after 24 hour incubation, the results found here are not in agreement with this [9]. However, the method Gotlink *et al*. used to measure the cellular sunitinib, is not similar to what was used here. The sunitinib-resistant HT-29 cells from Gotink *et al.* were continuously exposed to sunitinib and parental only for 24 hours before measuring the amount of sunitinib by liquid chromatography-tandem mass spectrometry (LC/MS-MS) analysis [9]. The procedure for flow cytometry performed here should probably have been executed differently. Here a 48 hours wash in drug-free medium was included prior to sunitinib incubation. This washing may have washed out the accumulated sunitinib in the HT-29/SR cells. A similar procedure as Gotink *et al*., where HT-29/SR cells are continuously exposed to sunitinib and HT-29/PAR only incubated for 24 hours, could have been employed instead. The same applies for the procedure used for fluorescence microscopy, where HT-29/SR cells were 24 hours in sunitinib-free medium followed by 24 hours sunitinib incubation. By changing the procedures, it would most likely have supported the assumption of sunitinib accumulation in HT-29/SR cells over time. However, an unanticipated result from these experiments is how quickly the clearance of sunitinib is, despite the 1-5 months continuous exposure of sunitinib, in HT-29/SR cells. The controls in flow cytometry (fig. 30) reveals only a slight difference between HT-29/PAR and HT-29/SR cells that have been incubated 48 hours in sunitinib-free medium.

However, it is also important to bear in mind that flow cytometry might not be a suitable method for quantification of the intracellular concentration of sunitinib. In endothelial cells, the uptake

of sunitinib can be observed as early as 10 seconds after exposure by fluorescence microscopy [95]. A 24 hours incubation of sunitinib as used in this thesis in both flow cytometry and fluorescence microscopy might have loaded the lysosomes to saturation, which can potentially lead to aggregation. Aggregation of sunitinib would have comprimised the fluorescence. This could be a feasible explanation for the large variation in sunitinib uptake within the cell lines by fluorescence microscopy, and could also explain why we do not detect a significant difference in cellular sunitinib between HT-29/PAR and HT-29/SR cells on flow cytometry. For future experiments, the amount of sunitinib that resides within the cells could be evaluated with a similar procedure executed by Gotlink et al. [9], where sunitinib is extracted from cell pellet homogenates and quantified.

A standard *in vitro* PCI procedure involves incubation of cells with the drug of interest prior to the photochemical treatment, the "light after"-procedure [84]. PCI is a drug delivery system that have shown to be feasible for both drug resistant and ROS- and radiation resistant cells [1]. Since sunitinib was shown to localized in lysosomes in both parental and sunitinib-resistant HT-29 cells, it was anticipated that PCI would be able to release sequestered drug and thereby induce toxicity in the cells. Sunitinib and $TPCS_{2a}$ was found to be localized in lysosomes, confirmed by co-localization with LysoTracker by fluorescence imaging in separate experiments in HT-29/PAR cells (fig. 29 and 31). In this study, PCI-mediated delivery of sunitinib to parental HT-29/PAR and HT-29/SR cells with "light after"-procedure was, however, not effective. The "light after"-procedure was also performed with red light as the absorption spectra implied that sunitinib could be excited by blue light. The antagonistic effect showed in preliminary PCI experiments with blue light, was, however, also found with red light. Nowak-Sliwinska *et al.* reported that sunitinib alone subjected to light at 420 ± 20 nm with a fluence rate of 200 mW/cm^2 for up to 5 minutes, which is equivalent to 60 J/cm^2, did not show significant changes in the absorption peaks [95]. This suggest that light exposure with blue light do not lead to structural changes or damage of the sunitinib molecules [95]. In this thesis red light was used in experiments involving sunitinib, to avoid light absorption by sunitinib itself.

It was therefore proposed that ROS generated by $TPCS_{2a}$ during photochemical reactions could destroy sunitinib, making it unable to exert its effect on the cells. The short half life of singlet oxygen means that sunitinib and $TPCS_{2a}$ had to be in close vicinity in order to obtain a photochemical destruction of sunitinib. Sunitinib has a log P value = 2,93-3,24 and $TPCS_{2a}$ log P = 3,65-4,69 [16, 40, 85]. The log P values of sunitinib and $TPCS_{2a}$ indicate that these

substances are lipophilic enough to confer endo/lysosomal membrane affinity. It is established that $TPCS_{2a}$ can reside in plasma and endo/lysosomal membranes [76, 77, 87]. Superresolution microscopy was here employed to investigate the intracellular localization of sunitinib and $TPCS_{2a}$. These images revealed co-localization of sunitinib and $TPCS_{2a}$, as hypothesized (fig. 36 and 37). Although the images were acquired without a marker for lysosomes, for instance LAMP or LysoTracker, they indicate that both sunitinib and $TPCS_{2a}$ are localized in the membrane of endo/lysosomes. Singlet oxygen can only diffuse about 10-20 nm in cellular environment, and the thickness of the membrane of lysosomes is in the range of 7-10 nm [18, 51]. Co-localization confirmed by superresolution microscopy suggests it is likely that ROS generated by excited $TPCS_{2a}$ can damage the sunitinib molecules. Another aspect that makes sunitinib susceptible for photochemical damage is the chemical structure (fig. 5). Sunitinib contains several functional groups that can induce photolability, including halogenated aromatic, carbonyl and nitroaromatic groups [61]. An *ex vivo* experiment with sunitinib and $TPCS_{2a}$ should be performed to further support this hypothesis of photochemical destruction of sunitinib upon the photochemical reaction.

Since there was a possibility for photochemical destruction of sunitinib, PCI with the "light first"-procedure was employed where the drug is administered immediately after light exposure [83]. This procedure induced higher toxicity than sunitinib and PDT alone in parental HT-29 cells (fig. 38). The same effect could not be observed with HT-29/SR cells. However, higher concentrations of sunitinib might be required for the PCI effect in HT-29/SR cells. This experiment was only performed once. It was attempted to reproduce these experiments, however due to time constraints and dettaching cells during the MTT assay it has not been successfully reproduced. Higher concentrations of sunitinib was used in "light first" experiments to evaluate if HT-29/SR cells respond to a "light first"-procedure, however, a new sunitinib stock was used during the end of the thesis which resulted in higher toxicity in the cells compared to the old stock at indicated sunitinib concentrations.

The results from the "light first"-procedure could indicate this as a potential strategy for intracellular drug delivery of sunitinib. In parental cells, a PCI effect could be observed at the lowest sunitinib concentration (1 μM) (fig. 37). The sunitinib concentrations used in the PCI experiments ranged from 1 μM to 8 μM, which are clinical relevant concentrations. The intratumoral concentration of sunitinib in patients receiving 37,5 to 50 mg/day have been found in the range of 5,1-13,4 μM [9]. Severe bleeding, disturbed wound healing and gastro-intestinal

perforation has been reported as side-effects for sunitinib [3, 7]. Since PCI of sunitinib in HT-29/PAR cells induced a larger reduction in viability compared to sunitinib and PDT alone, PCI with sunitinib can be a promising therapeutic strategy to increase sunitinib efficacy. $TPCS_{2a}$ is a clinical relevant PS that is currently evaluated in phase I/II studies (section 1.5.3). A lower dose of sunitinib could potentially reduce the risk of toxicity in these cancer patients.

The possible requirement for higher concentrations of sunitinib in HT-29/SR cells and the lack of a PCI effect with sunitinib and "light first" in the HT-29/SR cells implicates other resistance mechanisms than lysosomal sequestration to be involved in the sunitinib-resistance. The results further reject PCI as a suitable strategy to target the mechanism of resistance with the current procedure. However, when the cells were treated with PCI of rGel, a synergic response could be observed in both parental and sunitinib-resistant cells at the same rGel concentration and light dose indicating PCI of rGel as a feasible strategy to circumvent sunitinib resistance (fig. 41).

PCI of sunitinib and $TPCS_{2a}$ in HT-29/SR cells needs to be performed at higher concentration to explore if the "light first"-procedure is effective for sunitinib in sunitinib-resistant cells. It should be noticed that also, with the PCI "light first"-procedure of sunitinib, there was approximately 42 hours between plating in sunitinib-free medium to sunitinib exposure. The amount of sunitinib present in HT-29/SR cells at this point may have been minimal, according to the fluorecence intensisity found here by flow cytometry. For future experiments, a combination of "light first"- and "light after"-procedure could be employed, where HT-29/SR cells are continuously incubated with sunitinib from plating to the end of the experiment and receiving two cycles of illumination. The apparent antagonistic effect from light would complicate the analysis, but the experiment should be performed in order to conclude.

Although several methods used here, warrants optimalization we could not detect lysosomal sequestration of sunitinib in our resistant cells. Our results indicate that other mechanisms than lysosomal sequestration mediate the resistance in our research model. A defined cell line treated with a defined therapeutic agent can lead to the development of a heterogeneous range of drug-resistance mechanisms. It is possible that the mechanism causing resistance in our model is different than the model of Gotink *et al.* Furthermore, although Gotink *et al.* indeed showed lysosomal accumulation of sunitinib in their resistant cells, they did not prove this as the mechanism of resistance. It is therefore possible that other mechanisms are responsible for the resistance also in their system.

For future experiments, it would be interesting to study other sunitinib-resistant cell lines, and evaluate whether lysososmal sequestration is a relevant mechanism of sunitinib resistance. A sunitinib-resistant 786-O, renal cell adenocarcinoma, cell line have previously been established by Dr. Anette Weyergang at the Norwegian Radium Hospital, where the resistant cells were established using the same procedure as here (section 2.1). For future experimentation, this cell line should be included and evaluated for PCI of sunitinib since lysosomal sequestration has been postulated as a resistance mechanism also in these cells [9].

4.1 Sources of experimental errors

The methods used in this thesis can give rise to a range of potential sources of errors, which can have effected the results. Both random and systematic errors may have occurred during the experiments.

4.1.1 Experimental setup of flow and fluorescence microscopy

One of the weaknesses in these experiments, is the experimental setup in fluorescence microscopy and flow cytometry. By incubating the HT-29/SR cells in sunitinib-free medium, the accumulated sunitinib in these cells may have been cleared out and this may be why no difference in fluorescence could be observed between HT-29/PAR and HT-29/SR cells. The experiments should have been performed by continuous incubation of sunitinib in HT-29/SR cells, and further experiments with fluorescence microscopy and flow cytometry have to be employed in order to confirm the lysosomal accumulation by HT-29/SR cells. Cellular accumulated sunitinib should also be measured by extraction and monomerization in order to avoid false negative results due to aggregration.

4.1.2 Detaching cells during the MTT assay

Issues with detaching cells during incubation with MTT reagent was encoutered leading to loss of purple formazan crystals when removing medium. The procedure was changed during this thesis to avoid this. However, a few detaching cells were sporadically observed with the new procedure and could have resulted in overestimation of the toxicity, which can potentially be a problem for reproduction.

4.1.3 Sunitinib stock solution

The sunitinib stock solution used in this thesis was made in 2008. In the end of the thesis, a new stock solution was prepared and results from the experiments showed a substantially higher induction of toxicity in the cells than the previous stock. At 5 μM of sunitinib with the new solution, neither of the cell lines were viable, when tested with MTT assay. Whereas with the old stock, viable cells, in both cell lines, could be detected up to 10 μM. Most of the experiments with the new stock are exluded, however the old sunitinib stock solution represents a systematic source of error. For instance, the IC_{50} values found here are most likely overestimated due to a partly degraded stock solution. The effect of the new stock solution was evident with flow cytometry where the detected fluorescence intensity was 8 times stronger.

4.1.4 Subdued light during experiments

All the experiments with sunitinib and $TPCS_{2a}$ were perfomed under subdued light. However, it is possible that the PS could have been activated by unintentional light exposure. For PDT and PCI experiments, cells that were exposed to different light doses were seeded out in the same plate with one column apart. Dark controls were used to reduce the possibility of comparing samples that were exposed to unintentional light. Unintentional light exposure during PDT and PCI could result in data set indicating higher toxicity, and may be a problem for reproduction.

4.2 Future perspectives

The PCI experiments need to be reproduced in order to confirm or refute the "light first"-procedure as a drug delivery system of sunitinib in both HT-29/PAR and HT-29/SR cells. Lysosomal sequestration could not be observed as a resistance mechanism although lysosomal localization of sunitinib was found. More experiments are however needed to conclude here, including optimizing the procedures. A more mechanistic evaluation should be employed to evaluate the resistance mechanisms that have been induced by continuous exposure of sunitinib in our HT-29/SR cells. Provided that PCI of sunitinib with "light first"-procedure is feasible, *in vivo* studies would be relevant.

5 Conclusion

Development of drug resistance during treatment remains one of the leading causes for therapeutic failure despite major advances in the field of oncology the past decades. The resistance mechanisms are numerous and cancer cells can develop resistance to classes of cancer therapeutics that are structurally and mechanistically unrelated. PCI represent a drug delivery system for therapeutics trapped in endocytic vesicles. The scope of this thesis was to evaluate PCI as a drug delivery system of sunitinib in parental and sunitinib-resistant HT-29 cells. A sunitinib-resistant cell line was established in this thesis. The localization of sunitinib was confirmed by fluorescence microscopy in lysosomes, both in HT-29/PAR and HT-29/SR cells. More work is however needed to conclude lysosomal accumulation and the impact of this on sunitinib resistance. The results indicate that PCI of sunitinib with "light after"-procedure is not feasible in neither of the cell lines, where structural damage of sunitinib by ROS is proposed to be a cause. PCI of sunitinib was, however, indicated as highly effective using the "light first"-procedure in the HT-29/PAR cells. This effect could not be observed in HT-29/SR cells, although further experiments are required for optimalization of sunitinib doses in these cells in combination with PCI. The present thesis reject PCI as a mechanistic approach to overcome sunitinib resistance in our model. However, the sunitinib resistant cells were not found to be cross-resistant to PCI in general, and PCI of rGel is here indicated as a strategy to circumvent sunitinib resistance.

References

1. A. Weyergang, M. E. B. Berstad, B. Bull-Hansen, C. E. Olsen, P. E. Selbo and K. Berg, Photochemical activation of drugs for the treatment of therapy-resistant cancers. *Photochemical & Photobiological Sciences*, 2015, **14**(8), 1465-75.
2. B. Alberts, D. Bray, K. Hopkin, A. D. Johnson, J. Lewis, M. Raff, *et al.*, Essential cell biology. 3rd edition, New York: Garland Science, 2009, 555-568.
3. K. J. Gotink and H. M. Verheul, Anti-angiogenic tyrosine kinase inhibitors: what is their mechanism of action? *Angiogenesis*, 2010, **13**(1), 1-14.
4. CenterWatch, FDA Approved Drugs for Oncology. *Drug Information 2016*, 2016 [22.04 2016]; Available from: https://www.centerwatch.com/drug-information/fda-approved-drugs/therapeutic-area/12/oncology
5. J. Heidemann, D. G. Binion, W. Domschke and T. Kucharzik, Antiangiogenic therapy in human gastrointestinal malignancies. *Gut*, 2006, **55**(10), 1497-511.
6. S. Alexander and P. Friedl, Cancer invasion and resistance: interconnected processes of disease progression and therapy failure. *Trends in Molecular Medicine*, 2012, **18**(1), 13-26.
7. Statens Legemiddelverk (Norwegian Medicines Agency), Preparatomtale (SPC) Sutent, 2015 [31.08.2015; 22.02.2016]. Available from: http://www.ema.europa.eu/docs/no_NO/document_library/EPAR_-_Product_Information/human/000687/WC500057737.pdf
8. P. Carmeliet, Angiogenesis in life, disease and medicine. *Nature*, 2005, **438**(7070), 932-6.
9. K. J. Gotink, H. J. Broxterman, M. Labots, R. R. de Hass, H. Dekker, R. J. Honeywell, *et al*., Lysosomal sequestration of sunitinib: a novel mechanism of drug resistance. *Clinical Cancer Research*, 2011, **17**(23), 7337-46.
10. ATCC, HT-29 (ATCC® HTB-38™), [10.02.2016]. Available from: https://www.lgcstandards-atcc.org/products/all/HTB-38.aspx?geo_country=no&slp=1.
11. J. Zhou, Multi-drug resistance in cancer. *Springer Protocols*, New York: Humana Press, 2010, 1-6
12. M. M. Gottesman, T. Fojo and S. E. Bates, Multidrug resistance in cancer: role of ATP-dependent transporters. *Nature Reviews Cancer,* 2002, **2**(1), 48-58.

13. C. Holohan, S. V. Schaeybroeck, D. B. Longley and P. G. Johnston, Cancer drug resistance: an evolving paradigm. *Nature Reviews Cancer*, 2013, **13**(10), 714-26.
14. C. H. Choi, ABC transporters as multidrug resistance mechanisms and the development of chemosensitizers for their reversal. *Cancer Cell International,* 2005. **5**, DOI: 10.1186/1475-2867-5-30.
15. S. Shukla, Z. S. Chen and S. V. Ambudkar, Tyrosine kinase inhibitors as modulators of ABC transporter-mediated drug resistance. *Drug Resistance Updates*, 2012. **15**(1-2), 70-80.
16. B. Zhitomirsky and Y. G. Assaraf, Lysosomes as mediators of drug resistance in cancer. *Drug Resistance Updates*, 2016. **24**, 23-33.
17. P. Saftig and J. Klumperman, Lysosome biogenesis and lysosomal membrane proteins: trafficking meets function. *Nature Reviews Molecular Cell Biology*, 2009. **10**(9), 623-35.
18. H. Appelqvist, P. Wäster, K. Kågedal and K. Öllinger, The lysosome: from waste bag to potential therapeutic target. *Journal of Molecular Cell Biology*, 2013, **5**(4), 214-26.
19. T. Yamagishi, S. Sahni, D. M. Sharp, A. Arvind, P. J. Jansson and D. R. Richardson, P-glycoprotein mediates drug resistance via a novel mechanism involving lysosomal sequestration. *Journal of Biological Chemistry*, 2013, **288**(44), 31761-71.
20. B. Alberts, Molecular biology of the cell. 5th edition, New York, NY: Garland Science, 2008, 1218-22
21. D. Hanahan and R. A. Weinberg, Hallmarks of cancer: the next generation. *Cell*, 2011, **144**(5), 646-74.
22. S. M. Weis and D. A. Cheresh, Tumor angiogenesis: molecular pathways and therapeutic targets. *Nature Medicine*, 2011, **17**(11), 1359-70.
23. N. Ferrara, H.P. Gerber, and J. LeCouter, The biology of VEGF and its receptors. *Nature Medicine*, 2003, **9**(6), 669-76.
24. R. S. Kerbel, Tumor angiogenesis. *New England Journal of Medicine*, 2008, **358**(19), 2039-49.
25. L. Gossage, T. Eisen and E. R. Maher, VHL, the story of a tumour suppressor gene. *Nature Reviews Cancer*, 2015, **15**(1), 55-64.
26. R. M. Strieter, Masters of angiogenesis. *Nature Medicine*, 2005, **11**(9), 925-7.

27. J. E. Ziello, I. S. Jovin and Y. Huang, Hypoxia-Inducible Factor (HIF)-1 regulatory pathway and its potential for therapeutic intervention in malignancy and ischemia. *Yale Journal of Biology and Medicine*, 2007, **80**(2), 51-60.
28. A. P. Castano, T. N. Demidova and M. R. Hamblin, Mechanisms in photodynamic therapy: part one-photosensitizers, photochemistry and cellular localization. *Photodiagnosis and Photodynamic Therapy*, 2004, **1**(4), 279-93.
29. F. Broekman, E. Giovannetti and G.J. Peters, Tyrosine kinase inhibitors: Multi-targeted or single-targeted? *World Journal of Clinical Oncology*, 2011, **2**(2), 80-93.
30. J. G. Christensen, A preclinical review of sunitinib, a multitargeted receptor tyrosine kinase inhibitor with anti-angiogenic and antitumour activities. *Annals of Oncology*, 2007, **18**, DOI: 10.1093/annonc/mdm408
31. M. A. Lemmon and J. Schlessinger, Cell signaling by receptor tyrosine kinases. *Cell*, 2010, **141**(7), 1117-34.
32. J. Zhang, P. L. Yang and N. S. Gray, Targeting cancer with small molecule kinase inhibitors. *Nature Reviews Cancer,* 2009, **9**(1), 28-39.
33. E. Zwick, J. Bange and A. Ullrich, Receptor tyrosine kinase signalling as a target for cancer intervention strategies. *Endocrine-Related Cancer*, 2001, **8**(3), 161-173.
34. P. Wu, T. E. Nielsen and M. H. Clausen, FDA-approved small-molecule kinase inhibitors. Trends in Pharmacological Sciences, 2015, **36**(7), 422-39.
35. B. Alberts, Molecular biology of the cell. 6th edition, New York, NY: Garland Science, 2015, 1091-1127
36. K. Imai and A. Takaoka, Comparing antibody and small-molecule therapies for cancer. *Nature Reviews Cancer*, 2006. **6**(9), 714-27.
37. R. Munoz-Chapuli, A. R. Quesada and M. Angel Medina, Angiogenesis and signal transduction in endothelial cells. *Cellular and Molecular Life Sciences*, 2004, **61**(17), 2224-43.
38. S. Faivre, G. Demetri, W. Sargent and E. Raymond, Molecular basis for sunitinib efficacy and future clinical development. *Nature Reviews Drug Discovery*, 2007, **6**(9), 734-45.
39. H. L. Goel and A. M. Mercurio, VEGF targets the tumour cell. *Nature Reviews Cancer,* 2013, **13**(12), 871-82.
40. DrugBank, Sunitinib (DB01268), 2007 [05.01.2016; 06.01.2016]. Available from: http://www.drugbank.ca/drugs/DB01268

41. J. A. Engelman and J. Settleman, Acquired resistance to tyrosine kinase inhibitors during cancer therapy. *Current Opinion in Genetics & Development*, 2008, **18**(1), 73-9.
42. R. R. Allison, Photodynamic therapy: oncologic horizons. *Future Oncology*, 2014, **10**(1), 123-4.
43. P. Agostinis, K. Berg, K. A. Cengel, T. H. Foster, A. W. Girotti, S. O. Gollnick, *et al*., Photodynamic therapy of cancer: an update. *A Cancer Journal for Clinicians*, 2011, **61**(4), 250-81.
44. D. E. Dolmans, D. Fukumura, and R. K. Jain, Photodynamic therapy for cancer. *Nature Reviews Cancer*, 2003, **3**(5), 380-7.
45. M. R. Hamblin and Y. Huang, Handbook of photomedicine. Boca Raton, FL, CRC Press, 2014, 35-41, 11 and 386
46. D. Kessel, Introduction to photodynamic therapy. *Photobiological Sciences Online* (K. C. Smith, ed.), American Society for Photobiology, 2008 [29.03.2014; 10.04.2016]. Available from: http://photobiology.info/Kessel.html.
47. K. Berg, Photosensitizers in medicine, *Photobiological Sciences Online* (K. C. Smith, ed.), American Society for Photobiology, 2009 [11.11.2009; 15.02.2016]. Available from: http://photobiology.info/Berg.html.
48. Z. Huang, A review of progress in clinical photodynamic therapy. *Technology in Cancer Research & Treatment,* 2005, **4**(3), 283-93.
49. L. B. Josefsen and R.W. Boyle, Photodynamic therapy and the development of metal-based photosensitisers. *Metal-Based Drugs*, 2008, DOI: 10.1155/2008/276109
50. A. A. Rosenkranz, D. A. Jans and A. S. Sobolev, Targeted intracellular delivery of photosensitizers to enhance photodynamic efficiency. *Immunology & Cell Biology*, 2000, **78**(4), 452-64.
51. J. Moan and K. Berg, The photodegradation of porphyrins in cell can be used to estimate the lifetime of singlet oxygen. *Photochemistry and Photobiology,* 1991, **53**(4), 549-53.
52. K. Plaetzer, B. Krammer, J. Berlanda, F. Berr, T. Kiesslich, Photophysics and photochemistry of photodynamic therapy: fundamental aspects. *Lasers in Medical Science,* 2009, **24**(2), 259-68.

53. A. Juzeniene, K. P. Nielsen and J. Moan, Biophysical aspects of photodynamic therapy. *Journal of Environmental Pathology, Toxicology and Oncology*, 2006, **25**(1-2), 7-28.
54. R. R. Allison, G. H. Downie, R. Cuenca, X. H. Hu, C. J. Childs and C. H. Sibata, Photosensitizers in clinical PDT. *Photodiagnosis and Photodynamic Therapy*, 2004, **1**(1), 27-42.
55. A. B. Ormond and H. S. Freeman, Dye Sensitizers for Photodynamic Therapy. *Materials*, 2013, **6**(3), 817-40.
56. M. C. DeRosa and R. J. Crutchley, Photosensitized singlet oxygen and its applications. *Coordination Chemistry Reviews*, 2002, **233-234**, 351-71.
57. M. T. Huggett, M. Jermyn, A. Gilliams, R. Illing, S. Mosse, M. Novelli, *et al.*, Phase I/II study of verteporfin photodynamic therapy in locally advanced pancreatic cancer. *British Journal of Cancer*, 2014, **110**(7), 1698-704.
58. Aetna, Visudyne (Verteporfin) Photodynamic Therapy, 2002 [23.10.2015; 11.04.2016]. Available from: http://www.aetna.com/cpb/medical/data/500_599/0594.html.
59. Statens legemiddelverk (Norwegian Medicines Agency), Prepataomtale (SPC) Metvix, 2015 [27.11.2015; 09.04.2016]. Available from: http://slv.no/_layouts/Preparatomtaler/Spc/2001-08209.pdf
60. A. E. O'Connor, W. M. Gallagher and A. T. Byrne, Porphyrin and nonporphyrin photosensitizers in oncology: preclinical and clinical advances in photodynamic therapy. *Photochemical & Photobiological Sciences*, 2009, **85**(5), 1053-74.
61. H. H. Tønnesen, Photostability of drugs and drug formulations. 2nd ed, Boca Raton, FL, CRC Press, 2004, 21-27, 189-189.
62. R. A. Craig, C. P. McCoy, S. P. Gorman and D. S. Jones, Photosensitisers - the progression from photodynamic therapy to anti-infective surfaces. *Expert Opinion on Drug Delivery*, 2015, **12**(1), 85-101.
63. B. W. Henderson and T. J. Dougherty, How does photodynamic therapy work?. *Photochemistry and Photobiology*, 1992, **55**(1), 145-57.
64. A. Høgset, L. Prasmickaite, P. K. Selbo, M. Hellum, B. Ø. Engesaeter, A. Bonsted and K. Berg, Photochemical internalisation in drug and gene delivery. *Advanced Drug Delivery Reviews,* 2004, **56**(1), 95-115.

65. N. L. Oleinick, Basic photosensitization. *Photobiological Sciences Online* (K. C. Smith, ed.), American Society for Photobiology, 2010 [09.09.2011; 23.02.2016]. Available from: http://photobiology.info/Oleinick.html.

66. E. Buytaert, M. Dewaele and P. Agostinis, Molecular effectors of multiple cell death pathways initiated by photodynamic therapy. *Biochimica et Biophysica Acta*, 2007, **1776**(1), 86-107.

67. D. Kessel, M. G. Vicente and J. J. Jr. Reiners, Initiation of apoptosis and autophagy by photodynamic therapy. *Autophagy*, 2006, **2**(4), 289-90.

68. S. W. Ryter, K. Mizumura and A. M. Choi, The impact of autophagy on cell death modalities. *International Journal of Cell Biology*, 2014, article ID: 502676

69. Y. Liu and B. Levine, Autosis and autophagic cell death: the dark side of autophagy. *Cell Death & Differentiation*, 2015, **22**(3), 367-76.

70. A. P. Castano, P. Mroz and M.R. Hamblin, Photodynamic therapy and anti-tumour immunity. *Nature Reviews Cancer*, 2006, **6**(7). 535-45.

71. A. P. Castano, T. N. Demidova, and M.R. Hamblin, Mechanisms in photodynamic therapy: Part three-Photosensitizer pharmacokinetics, biodistribution, tumor localization and modes of tumor destruction. *Photodiagnosis and Photodynamic Therapy,* 2005, **2**(2), 91-106.

72. C. M. Brackett and S.O. Gollnick, Photodynamic therapy enhancement of anti-tumor immunity. *Photochemical & Photobiological Sciences*, 2011, **10**(5), 649-52.

73. Di. Yang, J. Savolainen, A. Jafarpous, D. Sprünken and J. L. Herek, A new paradigm for photodynamic therapy: coherent control.12th World Congress of the International Photodynamic Association, 11.-15.06.2009, Seattle, USA. [20.04.2016] Available from: http://os.tnw.utwente.nl/publications/books/yang1.pdf

74. K. C. Smith, Basic Photochemistry. *Photobiological Sciences Online* (K. C. Smith, ed.), American Society for Photobiology, 2009 [18.03.2014; 08.04.2016]. Available from: http://photobiology.info/Photochem.html

75. A. Mitra, C. H. Lee and K. Cheng, Advanced drug delivery, 1st edition, Hoboken, New Jersey, John Wiley & Sons Inc., 2014, 405-416

76. P. K. Selbo, A. Weyergang, A. Høgset, O. J. Norum, M. B. Berstad, M. Vikdal and K. Berg, Photochemical internalization provides time- and space-controlled endolysosomal escape of therapeutic molecules. *Journal of Controlled Release,* 2010, **148**(1), 2-12.

77. D. K. Adigbli and A. J. MacRobert, Photochemical internalisation: the journey from basic scientific concept to the threshold of clinical application. *Current Opinion in Pharmacology*, 2012, **12**(4), 434-8.

78. K. Berg, A. Weyergang, L. Prasmickaite, A. Bonsted, A. Høgset M. T. Strand, *et al.*, Photochemical internalization (PCI): a technology for drug delivery. *Methods in Molecular Biology,* 2010, **635**, 133-45.

79. A. Dietze, Q. Peng, P. K. Selbo, O. Kaalhus, C. Müller, S. Bown and K. Berg, Enhanced photodynamic destruction of a transplantable fibrosarcoma using photochemical internalisation of gelonin. *British Journal of Cancer*, 2005, **92**(11), 2004-9.

80. M. B. Berstad, L. H. Cheung, K. Berg, Q. Peng, A. S. Fremstedal, S. Patzke, *et al.*, Design of an EGFR-targeting toxin for photochemical delivery: in vitro and in vivo selectivity and efficacy. *Oncogene*, 2015, **34**(44), 5582-92.

81. O. J. Norum, J. V. Gaustad, E. Angell-Petersen, E. K. Rofstad, Q. Peng, K. E. Giercksky and K. Berg, Photochemical Internalization of Bleomycin is Superior to Photodynamic Therapy Due to the Therapeutic Effect in the Tumor Periphery. *Photochemistry and Photobiology,* 2009, **85**(3), 740-9.

82. P. J. Lou, P. S. Lai, M. J. Shieh, A. J. Macrobert, K. Berg and S. G. Bown, Reversal of doxorubicin resistance in breast cancer cells by photochemical internalization. *International Journal of Cancer*, 2006, **119**(11), 2692-8.

83. L. Prasmickaite, A. Høgset, P. K. Selbo, B. Ø. Engsaeter, M. Hellum and K. Berg, Photochemical disruption of endocytic vesicles before delivery of drugs: a new strategy for cancer therapy. *British Journal of Cancer*, 2002, **86**(4), 652-7.

84. K. Berg, A. Høgset, L. Prasmickaite, A. Weyergang, A. Bonsted, A. Dietze, *et al.,* Photochemical internalization (PCI): A novel technology for activation of endocytosed therapeutic agents. *Medical Laser Application*, 2006, **21**(4), 239-250.

85. M. Lilletvedt, H. H. Tønnesen, A. Høgset, S. A. Sande and S. Kristensen, Evaluation of physicochemical properties and aggregation of the photosensitizers TPCS2a and TPPS2a in aqueous media. *Pharmazie*, 2011, **66**(5), 325-33.

86. K. Berg, S. Nordstrand, P. K. Selbo, D. T. Tran, E. Angell-Petersen and A. Høgset, Disulfonated tetraphenyl chlorin (TPCS2a), a novel photosensitizer developed for clinical utilization of photochemical internalization. *Photochemical & Photobiological Sciences,* 2011, **10**(10), 1637-51.

87. J. T. Wang, K. Berg, A. Høgset, S. G. Brown and A. J. MacRobert, Photophysical and photobiological properties of a sulfonated chlorin photosensitiser TPCS(2a) for photochemical internalisation (PCI). *Photochemical & Photobiological Sciences*, 2013, **12**(3), 519-26.

88. I. Pastan, R. Hassan, D. J. FitzGerald and R. J. Kreitman, Immunotoxin therapy of cancer. *Nature Reviews Cancer*, 2006. **6**(7), 559-65.

89. M. D. Foster, A. Sultan, W. Jerjes, C. Simeon, S. Morley, D. Carnell and C. Hopper, First-in-man Phase I study of TPCS2a-based photochemical internalization (PCI) of bleomycin in locally recurrent or advanced/metastatic, cutaneous or subcutaneous malignancies. In: M. D. Foster, ESMO Congress 2012; 01.10.2012, Vienna, Austria [23.04.2016] Available from: http://www.poster-submission.com/cdrom/download_poster/33/22394/1061

90. F. Fan, M. F. McCarty, A. Belcheva, W. Liu, T. W. Bauer, R. J. Somcio, *et al*., Expression and function of vascular endothelial growth factor receptor-1 on human colorectal cancer cells. *Oncogene*, 2005, **24**(16), 2647-53.

91. PCI Biotech AS, LumiSource - novel light source for *'in vitro'* research. 2009 [12.12.2015]. Available from: http://pcibiotech.no/lumisource-novel-light-source-for-in-vitro-research/

92. T. L. Riss, R. A. Moravec, A. L. Niles, H. A. Benik, T. J. Worzella and L. Minor. Cell Viability Assays. *Assay Guidance Manual,* 2004 [29.06.2015; 22.01.2016]; Available from: http://www.ncbi.nlm.nih.gov/books/NBK144065/

93. S. P. Langdon, Cancer cell culture: methods and protocols, Methods in Molecular Medicine, Humana Press, 2004, **88**, 159-164.

94. N. A. P. Franken, H. M. Rodermond, J. Stap, J. Haverman and C. van Bree, Clonogenic assay of cells *in vitro. Nature Protocols,* 2006, **1**(5), 2315-9.

95. P. Nowak-Sliwinska, J. R. van Beijnum, T. J. Wong, W. W. Kilarski, G. Szweczyk, H. M. Verheul, *et al.*, Photoactivation of lysosomally sequestered sunitinib after angiostatic treatment causes vascular occlusion and enhances tumor growth inhibition. *Cell Death & Disease*, 2015, **6**, DOI: 10.1038/cddis.2015.4.

96. BD Biosciences, Introduction to Flow Cytometry: A Learning Guide. *Manual Part Number:11-11032-01* (BD Biosciences, ed.), 2000.

97. Thermo-Fischer Scientific, Introduction to Flow Cytometry. *Molecular Probes Tutorial Series* (Thermo-Fischer Scientific, ed.), 2014 [02.07.2014; 12.04.2016]

Available from:
https://www.thermofisher.com/no/en/home/support/tutorials.html#vid4

98. L. Chasin and D. Mowshowitz, Exponential growth. *Introduction to Molecular and Cellular Biology,* Colombia University NYC, 2000 [01.05.2016]. Available from: http://ccnmtl.columbia.edu/projects/biology/lecture1/expogrow.html

99. D. Ahmed, P. W. Eide, I. A. Eilertsen, S. A. Danielsen, M. Eknæs, M. Hektoen, *et al*., Epigenetic and genetic features of 24 colon cancer cell lines. *Oncogenesis*, 2013, **2**, DOI: 10.1038/oncsis.2013.35

100. J. Zhou, S. H. Tan, V. Nicolas, C. Bauvy, N. D. Yang, J. Zhang, *et al.*, Activation of lysosomal function in the course of autophagy via mTORC1 suppression and autophagosome-lysosome fusion. *Cell Research*, 2013, **23**(4), 508-23.

101. A. Weyergang, O. Kaalhus and K. Berg, Photodynamic targeting of EGFR does not predict the treatment outcome in combination with the EGFR tyrosine kinase inhibitor Tyrphostin AG1478. *Photochemical & Photobiological Sciences*, 2008, **7**(9), 1032-40.

Appendix

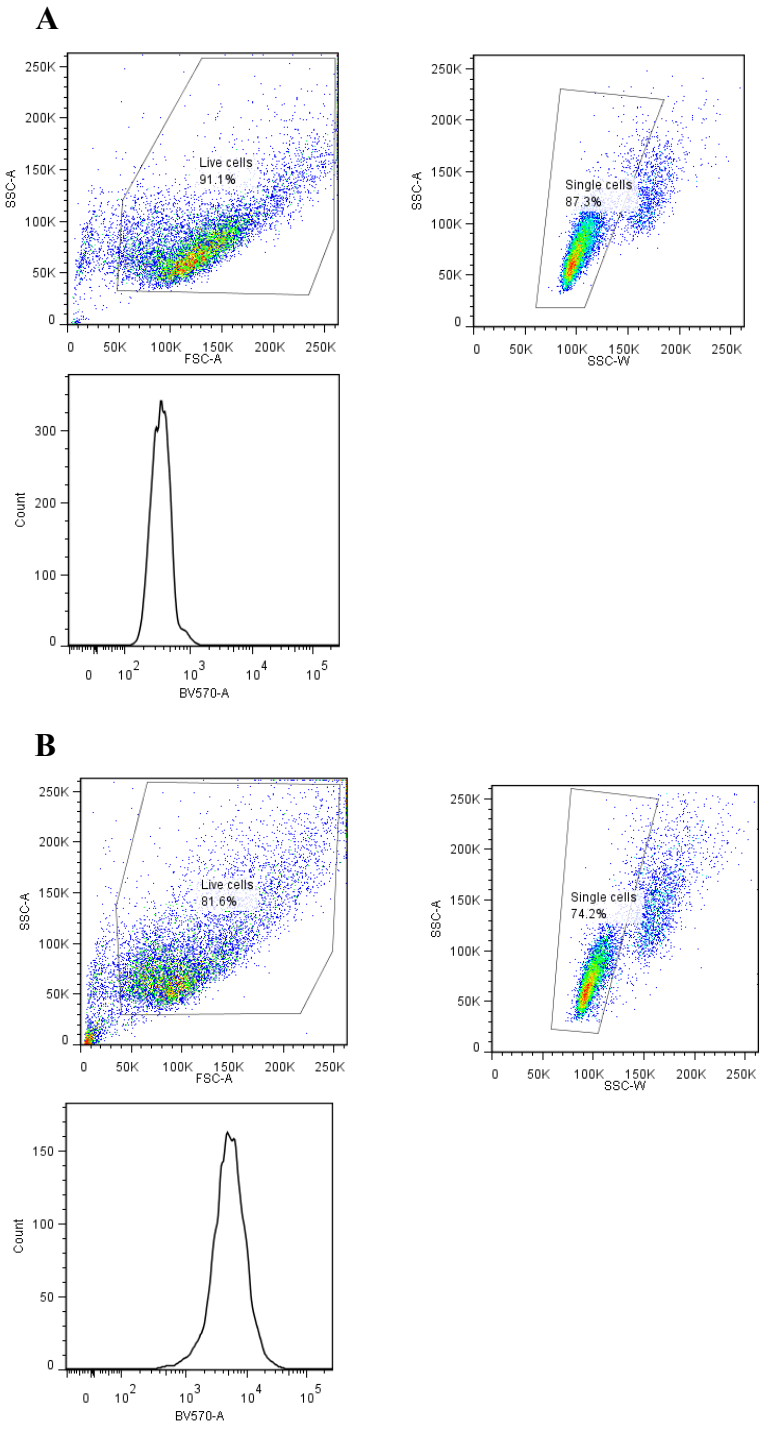

Flow cytometry: Representative flow chart of the gating (fig. 30) of HT-29/PAR cells where (A) is the control and (B) after 24 hours sunitinib incubation. SSC-A= Side-scattered light areal, SSC-W= Side-scattered light width, FSC-A= Forward-scattered light areal, BV570-A= Fluorescence intensity

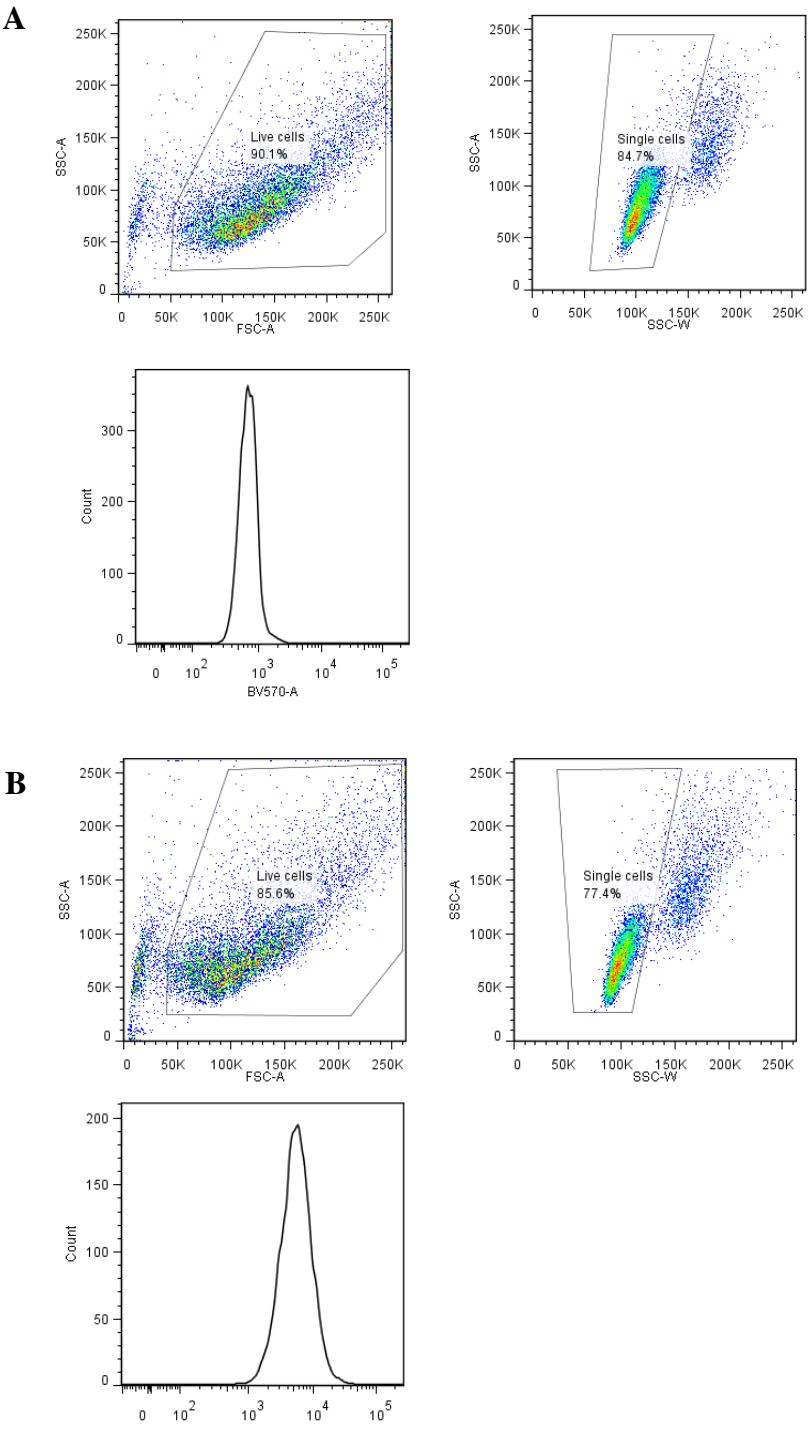

Flow cytometry. Representative flow chart of the gating (fig. 30) of HT-29/SR cells where (A) is the control and (B) after 24 hours sunitinib incubation. SSC-A= Side-scattered light areal, SSC-W= Side-scattered light width, FSC-A= Forward-scattered light areal, BV570-A= Fluorescence intensity